Journal of Electronic Imaging

JElectronicImaging.org

Multiobjective optimization for color display primary designs

Hao Xie
Carlos Eduardo Rodríguez-Pardo
Gaurav Sharma

SPIE. IS&T imaging.org

Hao Xie, Carlos Eduardo Rodríguez-Pardo, Gaurav Sharma, "Multiobjective optimization for color display primary designs," *J. Electron. Imaging* **26**(6), 063013 (2017), doi: 10.1117/1.JEI.26.6.063013.

Journal of Electronic Imaging 26(6), 063013 (Nov/Dec 2017)

Multiobjective optimization for color display primary designs

Hao Xie,* Carlos Eduardo Rodríguez-Pardo, and Gaurav Sharma
University of Rochester, Department of Electrical and Computer Engineering, Rochester, New York, United States

Abstract. The choice of primaries for a color display involves tradeoffs among different desirable attributes, such as a large color gamut, high spectral reproduction accuracy, minimal observer metamerism, and low power consumption. Optimization of individual attributes often drives primary choices in different directions. For example, expansion of color gamut favors narrow spectral bandwidth saturated primaries, and minimization of observer metamerism typically favors broadband primaries. We propose a multiobjective optimization framework to characterize the tradeoffs among the different attributes for three-primary and multiprimary displays. Instead of a single design, the framework determines the complete range of available primary choices that optimally negotiate the tradeoffs among the metrics for the different attributes. Using results obtained in our proposed framework, we explore the impact of the number of primaries, the relation between alternative design objectives, and the underlying primary spectral characteristics. For primary design and primary selection, the proposed strategy is more informative and comprehensive than alternative single objective optimization approaches. Furthermore, within the proposed framework, we also consider alternative strategies for selection of control values for multiprimary displays and demonstrate that we can better leverage the advantages of multiprimary displays by selecting the control strategy to align with desired objectives. Specifically, observer metamerism is significantly reduced if control values are selected to explicitly optimize multiobserver tristimulus accuracy. *© 2017 SPIE and IS&T* [DOI: 10.1117/1.JEI.26.6.063013]

Keywords: primary design; wide color gamut; observer metamerism; spectral reproduction; multiobjective optimization; Pareto optimization.

Paper 170448P received May 31, 2017; accepted for publication Oct. 9, 2017; published online Nov. 14, 2017.

1 Introduction

The design of the spectral power distribution (SPD) of the primaries plays a critical role in color display systems. The choice of primaries determines the display gamut, i.e., the range of colors that the display can reproduce. For example, to maximize the (chromaticity) gamut, the chromaticities of the RGB primaries in the recent Rec. 2020 standard[1] are defined such that they correspond approximately to spectrally monochromatic primaries with wavelengths of 630, 532, and 467 nm, respectively. An alternative strategy for realizing a wider gamut is to utilize more than three primaries, which is done in multiprimary displays. For both three-primary and multiprimary color displays, other display metrics such as luminance or power consumption also depend on the primaries characteristics. Practical display systems must therefore take into account these different performance attributes when in the primary design/selection process.

Prior work has considered several different metrics for evaluating a set of display primaries. Going beyond the consideration of only the two-dimensional (2-D) chromaticity gamut, several metrics have also been defined in terms of the SPDs of the primaries, and designs that optimize these metrics have also been obtained. Specifically, primary designs have been optimized for maximizing coverage of a prespecified target gamut volume[2,3] or absolute gamut volume in a perceptually uniform color space.[4] For wide gamut designs based on narrow spectral bandwidth primaries, observer metamerism is often a concern, and designs have been proposed to optimize spectral reproduction[5] and minimize observer metamerism.[6–8] These prior works, however, focus on a single objective to be optimized, and the question of how to adequately tradeoff these metrics against each other has received little attention. Primary designs have been proposed to mitigate the tradeoff between color gamut volume and optical power,[9,10] and between color gamut area and observer metamerism.[8] Alternatively, an importance-weighted optimization has also been proposed,[11] where the overall objective function for display primary design is formulated as a weighted sum of several metrics. However, the assignment of importance weights is empirical, and it is challenging to set the weights *a priori*, without knowing the nature of the interrelations among the different metrics.

In this paper, we propose a multiobjective/Pareto optimization framework to investigate the optimal tradeoff relations among different display metrics. Instead of a single design optimizing a numerical metric quantifying a single display trait (or a weighted combination), the Pareto optimization framework characterizes the complete set of solutions for which none of the metrics quantifying the different traits can be improved without compromising performance of at least one of the other metrics. As a result, instead of optimizing a single trait while disregarding all others, the Pareto optimal solution space fully characterizes the range of available primary choices that optimally negotiate the tradeoffs among the different traits for color displays. Using results

*Address all correspondence to: Hao Xie, E-mail: haoxie@rochester.edu

obtained in our proposed framework, we explore and quantify the impact of the number of primaries and the relation between alternative design objectives. For primary design/selection, the proposed strategy is more informative and comprehensive. Furthermore, within the proposed framework, we also consider alternative strategies for selection of control values for multiprimary displays and demonstrate that we can better leverage the advantages of multiprimary displays by selecting the control strategy to align with desired objectives. Specifically, compared to alternative approaches, observer metamerism can be significantly reduced via the selection of control values to explicitly optimize multiobserver tristimulus accuracy.

Preliminary results from the research presented here were featured in a paper[12] presented at the 2017 Electronic Imaging symposium. This paper is more comprehensive and considers more effective approaches for color conversion.

This paper is organized as follows. Section 2 lays the mathematical foundation for our problem setting by introducing spectral models for the display system and for object colors and their interrelations via colorimetric/spectral reproduction objectives. In Sec. 3, metrics quantifying the display attributes of color gamut coverage, power consumption, and observer metamerism are defined and the multiobjective optimization problem is formulated in terms of these metrics. Section 4 describes our implementation of the Pareto optimization framework using a parameterized representation of the primaries for computational efficiency and Sec. 5 summarizes the simulation parameters and settings used for our study. Results obtained using the framework are presented in Sec. 6, where the nature of the optimal tradeoff relations and the underlying spectral properties of the primaries are discussed. A discussion of the results and summary of the conclusions form Secs. 7 and 8. Appendices A and B provide details of the color conversion approach and the gamut mapping method used in our work.

2 Preliminaries

To provide a foundation for the proposed formulation, we summarize the required background information in this section. We introduce a spectral model for the display, discuss spectral and color representations for the surface colors that the display seeks to reproduce, and discuss the color conversion process for the display, whereby control values for the primaries are determined, taking into account colorimetric and spectral reproduction objectives. Anticipating the interest in observer metamerism, the discussion of color representations also covers observer variability.

2.1 *Display and Object Spectral Distributions*

For a display system with K ($K \geq 3$) primaries, we model the spectrum rendered by the display in terms of the K primary spectra and their specified control values as

$$S_d(\lambda) = \sum_{i=1}^{K} \alpha_i p_i(\lambda) + p_0(\lambda), \tag{1}$$

where $p_i(\lambda)$ is the spectrum of the i'th ($1 \leq i \leq K$) primary, α_i, $0 \leq \alpha_i \leq 1$, is the corresponding control value, and $p_0(\lambda)$ is the display black spectrum emitted when all primary control values are set to 0. The display black spectrum $p_0(\lambda)$ arises from the combination of reflected ambient light as well as from "leakage" light emitted by the display. We also refer to $p_0(\lambda)$ as flare regardless of its source. Note that $S_d(\lambda)$ is a function of the control values α_i, and thus, in the cases when this dependency needs to be highlighted, we opt for the more explicit notation $S_d(\lambda; \alpha_1, \ldots, \alpha_K)$.

Object stimuli that the display is expected to emulate and reproduce are modeled as the product of the illuminant spectrum and the object reflectance. That is, the spectrum for an object stimulus is given by $S_o(\lambda) = l(\lambda)r(\lambda)$, where $l(\lambda)$ is the illuminant SPD and $r(\lambda)$ is the spectral reflectance of the object.

2.2 *Color Representation*

Given the stimulus SPD, a color representation can be determined as a tristimulus vector $\mathbf{c} = [X, Y, Z]^T$ computed using the observers' cone sensitivities, or more commonly XYZ color matching functions (CMFs), $x(\lambda)$, $y(\lambda)$, and $z(\lambda)$, as

$$\begin{aligned} X &= \int x(\lambda)S(\lambda)\mathrm{d}\lambda, \\ Y &= \int y(\lambda)S(\lambda)\mathrm{d}\lambda, \\ Z &= \int z(\lambda)S(\lambda)\mathrm{d}\lambda, \end{aligned} \tag{2}$$

where $S(\lambda)$ can be either the display output spectrum $S_d(\lambda)$ or the object spectrum $S_o(\lambda)$, and the superscript T denotes the transpose operation. Standardized versions of the CMFs denoted as $\bar{x}(\lambda)$, $\bar{y}(\lambda)$, and $\bar{z}(\lambda)$ are defined by the CIE[13] as representative averages. The corresponding tristimulus values are then referred to as the CIEXYZ tristimulus values. Alternative color space representations, specifically, approximately perceptually uniform CIE $u'v'$ chromaticities and CIELAB values, can then be obtained from these tristimulus values using standard transformations.[13] To account for the individual differences in cone sensitivities, i.e., the phenomena of observer metamerism, we also consider Eq. (2) for a population of M observers characterized by their individual CMFs, $x_j(\lambda)$, $y_j(\lambda)$, and $z_j(\lambda)$ ($1 \leq j \leq M$).

We denote by $\mathbf{p}_0, \mathbf{p}_1, \ldots, \mathbf{p}_K$ the CIEXYZ tristimulus values corresponding, respectively, to the SPDs $p_0(\lambda)$, $p_1(\lambda), \ldots, p_K(\lambda)$ that represent the display flare and the K display primaries. The $3 \times K$ matrix $\mathbf{P} = [\mathbf{p}_1, \mathbf{p}_2, \ldots, \mathbf{p}_K]$ then represents the matrix of the primary tristimulus vectors.

2.3 *Display Color Conversion*

Color conversion is the process of determining primary control values $\alpha_1, \alpha_2, \ldots, \alpha_K$ for reproducing a target color or spectral stimuli. The color conversion process also impacts a number of display performance attributes, in addition to the choice of the display spectra. For instance, for the same choice of display primary spectra, different methodologies of color conversion can lead to different degrees of observer metamerism. Also, for technologies such as OLED, where each pixel individually contributes to power consumption (rather than a fixed backlight), the approach used to determine the control values also determines the display power consumption. Therefore, when considering the design of the display primary SPDs, it is critical to also take into account the color conversion approach used. To assess the

impact of the display color conversion approach, here we consider four alternative approaches, which focus on colorimetric reproduction, spectral reproduction, a combination of the two, or multiobserver tristimulus accuracy.

2.3.1 *Colorimetric matching for standard observer*

The conventional objective of color reproduction is to match the colorimetry for the standard observer. That is to reproduce an object stimulus $S_o(\lambda)$, one aims to produce a display spectrum $S_d(\lambda)$ such that their CIEXYZ tristimulus values match for the standard observer. This criterion is referred to as an absolute colorimetric match, as opposed to a relative colorimetric match that is more commonly used.[14] Also, the object stimulus is often only specified in terms of a colorimetric rather than spectral representation. We use the spectral representation as the basis because observer metamerism is a specific focus of our investigation. Mathematically, if $\mathbf{c} = [X_o, Y_o, Z_o]^T$ is the 3×1 vector of CIEXYZ tristimulus values for corresponding to the object stimulus $S_o(\lambda)$, the objective of colorimetric matching is to determine a feasible control value vector $\boldsymbol{\alpha} = [\alpha_1, \alpha_2, \ldots, \alpha_K]^T$ such that

$$\mathbf{c} = \mathbf{p}_0 + [\mathbf{p}_1, \mathbf{p}_2, \ldots, \mathbf{p}_K]\boldsymbol{\alpha} = \mathbf{p}_0 + \mathbf{P}\boldsymbol{\alpha}, \tag{3}$$

where feasible means that $0 \le \alpha_i \le 1$, for all $i = 1,2,\ldots,K$. The set of CIEXYZ values for which the display can produce a colorimetric match (with feasible control values) is called the display (CIEXYZ) gamut. For three primaries displays, there is a unique triplet of control values that produces each tristimulus contained in the gamut. Multiprimary displays provide flexibility for colorimetric reproduction; for tristimulus values that lie inside the display gamut, there are multiple control values that yield spectral responses with matching colorimetry. (Tristimuli lying on the gamut boundary have uniquely determined control values whereas for tristimuli that are strictly inside the gamut there are multiple control values.)

To determine control values for multiprimary displays, additional constraints or considerations are typically introduced to choose between the multiple sets of control values that can reproduce a given color.[15–20] Because of its relative computational simplicity, we consider the colorimetric matching using the matrix switching (CMMS)[15] approach in our study. The CMMS strategy is based on a gamut partition into nonoverlapping quadrangle pyramids corresponding to facets of the CIE XYZ tristimulus gamut, within each of which, the strategy determines a unique set of feasible control values using the pyramidal representation. The method effectively switches between using alternative 3×3 matrices associated with each pyramid for the color conversion, and this switching gives the strategy its name. For completeness, and because we leverage some of the attractive characteristics of the CMMS approach to address out of gamut colors in our methodology, we provide a complete description of the CMMS implementation in Appendix A.

2.3.2 *Spectral approximation under colorimetric matching*

As an alternative to the CMMS approach, the flexibility in the choice of control values for multiprimary displays can also be beneficially exploited to improve display performance attributes that are not directly a function of the colorimetry. A particularly useful approach is to determine the control values to minimize the spectral reproduction error while maintaining the colorimetric match desired. This approach has the advantage that it integrates the dual goals of spectral reproduction[5,21] and colorimetric reproduction, and the improved spectral accuracy reduces the impact of observer metamerism. Specifically, we consider the approach of spectral approximation under colorimetric matching (SACM) for the standard observer,[22] where the control values are determined as the solution to the following optimization:

$$\begin{aligned}
&\underset{\alpha_1,\ldots,\alpha_K}{\text{minimize}} \left\| S_d(\lambda;\alpha_1,\ldots,\alpha_K) - S_o(\lambda) \right\|_2^2 \\
&\text{subject to } 0 \le \alpha_i \le 1, \quad i = 1,\ldots,K \\
&\int \bar{x}(\lambda) S_o(\lambda) \mathrm{d}\lambda = \int \bar{x}(\lambda) S_d(\lambda) \mathrm{d}\lambda \\
&\int \bar{y}(\lambda) S_o(\lambda) \mathrm{d}\lambda = \int \bar{y}(\lambda) S_d(\lambda) \mathrm{d}\lambda \\
&\int \bar{z}(\lambda) S_o(\lambda) \mathrm{d}\lambda = \int \bar{z}(\lambda) S_d(\lambda) \mathrm{d}\lambda.
\end{aligned} \tag{4}$$

The optimization problem is convex and can in fact be shown to correspond to a quadratic objective function in the control values with linear equality and inequality constraints.[22] Thus, there is a unique local optimum that is also the global optimum and the minimizer can be readily computed using numerical optimization techniques.[23]

2.3.3 *Multiobserver tristimulus approximation*

In a framework very similar to SACM, one can also consider an alternative approach that determines display control values to directly reduce observer metamerism.[22] Specifically, given the individual CMFs, $x_j(\lambda)$, $y_j(\lambda)$, and $z_j(\lambda)$ $(1 \le j \le M)$, for a population of M observers, the control values for reproducing a given target spectrum $S_o(\lambda)$ can be determined so as to minimize the total mean-squared tristimulus error between the target and display reproduction for the M observers while requiring a colorimetric match for the standard observer. Mathematically, the control values are obtained as

$$\begin{aligned}
&\underset{\alpha_1,\ldots,\alpha_K}{\text{minimize}} \sum_{j=1}^{M} \left\| \mathbf{c}_o^j - \mathbf{c}_d^j \right\|_2^2 \\
&\text{subject to } 0 \le \alpha_i \le 1, \quad i = 1,\ldots,K \\
&\int \bar{x}(\lambda) S_o(\lambda) \mathrm{d}\lambda = \int \bar{x}(\lambda) S_d(\lambda) \mathrm{d}\lambda \\
&\int \bar{y}(\lambda) S_o(\lambda) \mathrm{d}\lambda = \int \bar{y}(\lambda) S_d(\lambda) \mathrm{d}\lambda \\
&\int \bar{z}(\lambda) S_o(\lambda) \mathrm{d}\lambda = \int \bar{z}(\lambda) S_d(\lambda) \mathrm{d}\lambda,
\end{aligned} \tag{5}$$

where $\mathbf{c}_o^j = [X_o^j, Y_o^j, Z_o^j]^T$ and $\mathbf{c}_d^j = [X_d^j, Y_d^j, Z_d^j]^T$ are the tristimulus vectors of target spectrum $S_o(\lambda)$ and the displayed spectrum $S_d(\lambda;\alpha_1,\ldots,\alpha_K)$, respectively, for the j'th observer.

We refer to this approach as multiobserver tristimulus approximation (MOTA), where the constraint of colorimetric matching can be seen as an ideal approximation for the standard observer. The optimization problem in Eq. (5) is analogous to the SACM problem in Eq. (4) with a change of the objective function. It can be readily seen that Eq. (5) also corresponds to a quadratic objective function in the control values with linear equality and inequality constraints.[22] A solution can therefore be readily obtained numerically.

2.3.4 *Spectral least squares minimization*

The SACM and MOTA approaches can be computationally demanding, especially when used in optimizing primary SPDs. Alternatively, we also consider a more computationally efficient approach that minimizes spectral error without giving any consideration to colorimetry. In this naive spectral approximation (NSA) method, the control values for (approximately) reproducing a target spectral stimuli $S_o(\lambda)$ are determined by solving the optimization problem

$$\underset{\alpha_1,\ldots,\alpha_K}{\text{minimize}} \|S_d(\lambda;\alpha_1,\ldots,\alpha_K) - S_o(\lambda)\|_2^2$$
$$\text{subject to } 0 \le \alpha_i \le 1, \quad \text{for } i = 1,\ldots,K. \tag{6}$$

This approach has previously been used in optimizing display primary design for minimizing observer metamerism[8] and was also used in our preliminary work.[12]

2.3.5 *Gamut mapping*

The CMMS, SACM, and MOTA methods are applicable for colors inside the display gamut. Colors outside the display gamut need to be first mapped inside the gamut for the methods to be used. This step cannot be ignored in the proposed work because when searching over the space of alternative primary designs, it is impractical to assume that the colors targeted for reproduction will all be within the gamut. We adopt a simple approach that approximately preserves CIELUV hue and advantageously exploits the characteristics of the CMMS approach. Out of gamut colors are gamut mapped via a two-stage process whose principal idea we outline here and provide details in Appendix B. First, unless it is already inside, the chromaticity is remapped along the constant-hue radial line in the CIE $u'v'$ diagram to the (approximate) boundary of the $u'v'$ chromaticity gamut, keeping the luminance unchanged. Next, if the CIEXYZ tristimulus value obtained from the first stage is outside the gamut volume, it is scaled (after subtraction of the display black luminance that acts as an offset) by a factor that ensures that the resulting gamut mapped tristimulus value lies on the gamut surface. The latter step approximately preserves chromaticity and is advantageously enabled by the characteristics of the CMMS method, as detailed in Appendix B.

We adopt this relatively simple gamut mapping approach for its low computational simplicity, which is advantageous given that multiobjective optimization is fairly computationally demanding. Once the display design is complete, more sophisticated gamut mapping techniques[24,25] can be utilized. Specifically, the final gamut mapping approach used in practice is not constrained to hard clipping at the gamut boundaries and the nonideal hue approximation in $u'v'$ chromaticity that are used in our simple gamut mapping approach.

2.4 *Display White and Flare*

The white stimulus plays a critical role in color reproduction, in particular, in determining the viewer's state of adaptation. Traditionally, the spectrum in Eq. (1) with all control values α_i set to unity, i.e., maximum is considered as the display white and the chromaticity of this spectrum is constrained to match a specified white chromaticity and the corresponding luminance then determines the display's dynamic range. However, having a predetermined specification of the white in this manner conflicts with the spectral and multiobserver tristimulus reproduction objectives that we use in this paper. We therefore define the white spectrally by the illuminant SPD $l(\lambda)$. This assumption has also been adopted in other recent works,[8] considering observer metamerism for multiprimary displays.

The impact of the display flare, modeled in Eq. (1) by the term $p_0(\lambda)$, is determined by its magnitude relative to the white stimulus. We assume that the flare $p_0(\lambda)$ is modeled as a fraction κ of the sum of the primaries, i.e.,

$$p_0(\lambda) = \kappa \sum_{i=1}^{K} p_i(\lambda), \tag{7}$$

where the scaling factor κ is determined to set the flare luminance Y_0 to a fraction ζ of the white luminance Y_W (computed for the standard observer). It can be readily seen that $\kappa = \zeta Y_W/(\sum_i Y_i)$ where Y_i denotes the luminance corresponding to the i'th primary $p_i(\lambda)$. This modeling procedure allows us to represent a consistent level of flare as the primary spectra vary while still providing a spectral representation for the flare, which is necessary for our consideration of spectral reproduction and observer metamerism. Strictly speaking, Eq. (7) models primary "leakage," whereas the flare also includes additional components such as reflected ambient light. However, we simplify and use Eq. (7) to model the complete flare. This simplification is justified because under typical situations, where the luminance level of the flare is relatively low ($\zeta \ll 1$), the chromaticity gamut coverage is critically impacted by the factor ζ (as discussed and shown in Sec. 3.1.1) but is largely insensitive to the exact spectral composition of the flare.

3 Problem Formulation

For presenting concrete Pareto optimal formulations and designs, in this paper, we use three important display metrics quantifying color gamut coverage, power consumption, and observer metamerism, respectively. The proposed Pareto framework can readily include additional metrics defined in terms of the specified display parameters.

3.1 *Display Metrics*

3.1.1 *Color gamut coverage*

The color gamut for a display system is defined as the set of all tristimulus values for the display spectra $S_d(\lambda)$ in Eq. (1) as the control values α_i vary over their feasible ranges between 0 and 1. Because the tristimulus space is not perceptually uniform, alternative gamut representations in perceptual spaces are usually considered for display design. Specifically, we quantify the color gamut by the approximate gamut area coverage in the CIE $u'v'$ uniform chromaticity

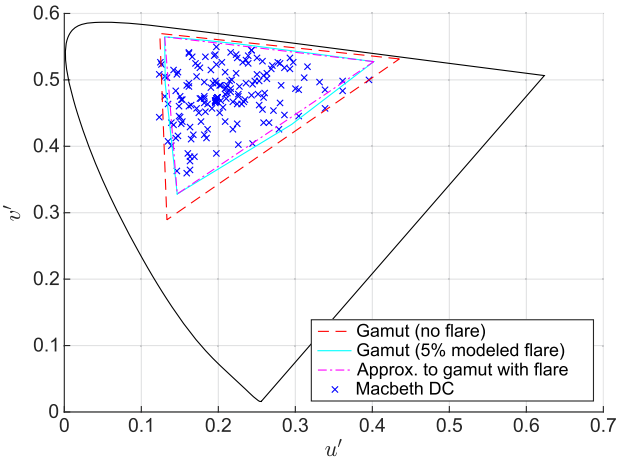

Fig. 1 Example illustrating the gamut coverage metric $\mathcal{G}_{uv}$ for a sample three-primary display on the CIE $u'v'$ chromaticity diagram. The chromaticities for the three primaries are the vertices of the red triangle. The flare, set to an exaggerated 5% [$\zeta = 0.05$ in Eq. (7)] level for clearer illustration, reduces the saturation of the primaries, moving them to the vertices of the smaller magenta triangle. The actual chromaticity gamut area coverage for the design is the area enclosed in the cyan closed curve, but for computational simplicity we approximate the gamut area coverage as the area $\mathcal{G}_{uv}$ enclosed by the magenta triangle. The blue cross marks correspond to 172 object colors from the Macbeth DC color checker under the CIE D65 illuminant (redundant neutral colors and glossy patches are excluded).

scale.[13] Channel chromaticities are defined as the $u'v'$ chromaticities corresponding to the tristimuli $\mathbf{p}_i + \mathbf{p}_0$, for $i = 1,2,\ldots,K$; which represent the individual primary channels in the presence of flare. We quantify the color gamut coverage as the area $\mathcal{G}_{uv}$ of the convex polygon formed with the K channel chromaticities as the vertices. We note that due to the flare, the channel chromaticities are desaturated in comparison to the primary chromaticities for the tristimuli $\mathbf{p}_i$, for $i = 1,2,\ldots,K$, and, in fact, the actual display chromaticity gamut is slightly larger than our estimate. For typical levels of flare, the difference is relatively minor. Figure 1 shows an example of our gamut coverage metric for a three-primary display, where a rather high level (5%) of flare is used to clearly distinguish among the different plots. The area of the magenta triangle whose vertices are defined by the three channel chromaticities represents the gamut coverage metric $\mathcal{G}_{uv}$ that we use. Also included in Fig. 1 are the chromaticity coordinates of the patches in the Macbeth DC color checker (under the CIE D65 illuminant) reflecting the coverage of these in the gamut. We note that it is important to take flare into consideration in defining the metric $\mathcal{G}_{uv}$ in order to avoid numerical instability: in the absence of flare, an infinitesimal power allocation to a primary can cause a significant increase in the chromaticity gamut coverage.

We note that our choice of a 2-D gamut area coverage is motivated by computational simplicity. Although, three-dimensional (3-D) gamut volume in a perceptually uniform color space can be computed efficiently,[26] the calculations still pose a rather high computational burden for the multiobjective optimization framework. Additionally, the luminance dimension is in part implicitly considered in our metric because, in the presence of the flare, the luminance of primaries impacts the chromaticity gamut area $\mathcal{G}_{uv}$.

3.1.2 *Power consumption*

Power consumption is an important consideration for displays, particularly for battery-powered mobile devices, where the display is responsible for a substantial part of the total power use. As a proxy for the electrical power, we use the optical power, which is directly computable from the primary SPDs. Specifically, the optical power of the i'th primary is obtained as

$$\mathcal{P}_i = \int p_i(\lambda)\mathrm{d}\lambda, \tag{8}$$

and the total optical power consumed when all primaries are at their maximum amplitudes is then

$$\mathcal{P}_{\max} = \sum_{i=1}^{K} \mathcal{P}_i, \tag{9}$$

where we have ignored the optical power for the display flare. Note that for displays based on the modulation of a constant backlight, such as most of LCD displays, the power $\mathcal{P}_{\max}$ represents the total power consumed any time the display is powered on, independent of what is displayed. In contrast, for displays that directly modulate their primaries, such as OLEDs, the optical power for reproducing a spectrum $S_d(\lambda)$ depends on the control values as

$$\mathcal{P}_{s_d} = \sum_{i=1}^{K} \alpha_i \mathcal{P}_i. \tag{10}$$

The power consumption of displays that directly modulate their primaries is therefore determined by the strategy used to determine control values as well as by the distribution of colors reproduced. As an alternative to one of the color conversion strategies we consider, display control values for these scenarios can be alternatively optimized to minimize power consumption under a colorimetric match. For simplicity, we use $\mathcal{P}_{\max}$ as our power metric, which, for all types of displays, represents an upper bound for the optical power.

3.1.3 *Observer metamerism*

Given that most displays are designed with three relatively broadband primaries, observer metamerism has not been widely considered in the process of display design. However, with the emergence of wide color gamut displays using narrow band primaries, the phenomenon of observer metamerism is gaining more attention.[6] The index of observer metamerism magnitude[27,28] $\mathcal{M}_O$ aligns well with our established objective of spectral reproduction, and we therefore adopt it as the metric for the quantification of observer metamerism instead of the more traditional CIE metamerism index.[29]

The computation of observer metamerism index considers a pool of M available observers, represented by their CMFs, $x_j(\lambda)$, $y_j(\lambda)$, and $z_j(\lambda)$, $j = 1,\ldots,M$, and a set of N object samples represented by the SPD $S_{o,n}(\lambda)$, $n = 1,\ldots,N$. For the j'th observer, we denote by $\Delta E_{j,n}$ the Euclidean distance between the CIELAB color space representations of the n'th object spectrum $S_{o,n}(\lambda)$ and the corresponding display

reproduced spectrum $S_{d,n}(\lambda)$ on the display. The display performance for the observer is quantified by the average error

$$\overline{\Delta E_j} = \frac{1}{N}\sum_{n=1}^{N} \Delta E_{j,n}. \tag{11}$$

The observer metamerism index $\mathcal{M}_O$ is then defined as the worst reproduction error across all the observers, that is,

$$\mathcal{M}_O = \max_{j=1,\ldots,M} \overline{\Delta E_j}. \tag{12}$$

3.2 *Multiobjective Optimization Problem*

Having defined the display metrics under consideration, we formulate the problem of designing the primary spectra as a multiobjective optimization problem (MOOP),[30] aiming to examine the optimal tradeoffs between display metrics defined previously. Specifically, the optimal designs are a solution set for the following problem:

$$\begin{aligned} &\underset{p_1(\lambda),p_2(\lambda),\ldots,p_K(\lambda)}{\text{maximize}} \{\mathcal{G}_{uv}, -\mathcal{M}_O, -\mathcal{P}_{\max}\} \\ &\text{subject to } p_i(\lambda) \geq 0, \quad i = 1,2,\ldots,K \\ &p_0(\lambda) = \kappa \sum_{i=1}^{K} p_i(\lambda), \end{aligned} \tag{13}$$

where the constraints are set to guarantee physically realizable primaries with nonnegative SPDs and specify the amount of the flare in terms of its luminance ζY_W.

4 MOOP Implementation Using Parameterized Primaries

To obtain and analyze Pareto optimal designs for our MOOP formulation in Eq. (13), we consider a parameterization of the display design space as follows. Each primary SPD, $p_i(\lambda)$, is parameterized as a Gaussian function

$$p_i(\lambda) = \frac{\gamma_i}{\sqrt{2\pi\sigma_i^2}} \exp\left[-\frac{(\lambda-\mu_i)^2}{2\sigma_i^2}\right], \tag{14}$$

where parameter μ_i is the location of the peak wavelength, σ_i is the standard deviation quantifying the spectral width as the half-width at $e^{-(1/2)} \approx 0.607$ of the peak amplitude, and γ_i is the primary amplitude. An advantageous feature of this parameterization[4] is that the optical power is immediately obtained as

$$\mathcal{P}_i = \int p_i(\lambda)\mathrm{d}\lambda = \gamma_i. \tag{15}$$

With this parameterization, the solution space of the optimization problem defined in Eq. (13) reduces to a $3K$-dimensional space defined by the parameters $(\mu_i, \sigma_i, \gamma_i)$ for each of the K primaries. Specifically, in the parameterized space, for our computational evaluations, we use the MOOP formulation

$$\begin{aligned} &\underset{\mathbf{t}}{\text{maximize}} \{\mathcal{G}_{uv}, -\mathcal{M}_O, -\mathcal{P}_{\max}\} \\ &\text{subject to } a_\sigma \leq \sigma_i \leq b_\sigma, \quad 1 \leq i \leq K \\ &\quad a_\mu \leq \mu_i \leq b_\mu, \quad 1 \leq i \leq K \\ &\quad 0 \leq \gamma_i, \quad 1 \leq i \leq K \\ &\quad E_B^{(L)} \leq \sum_{i=1}^{K} \gamma_i \leq E_B^{(U)} \\ &\quad p_0(\lambda) = \kappa \sum_{i=1}^{K} p_i(\lambda), \end{aligned} \tag{16}$$

where $\mathbf{t} = [\mu_1,\ldots,\mu_K,\sigma_1,\ldots,\sigma_K,\gamma_1,\ldots,\gamma_K]$ is a $3K$-dimensional vector of K-primary display parameters with $\mu_1,\ldots,\mu_K$ representing peak wavelengths, $\sigma_1,\ldots,\sigma_K$ representing spectral widths for the Gaussian SPDs, and $\gamma_1,\ldots,\gamma_K$ representing the relative primary optical power levels. The constraints include lower bounds, a_μ and a_σ, and upper bounds, b_μ and b_σ, for the peak wavelengths and spectral widths, and $E_B^{(L)}$ and $E_B^{(U)}$ represent the range of power budget explored in the design space in units consistent with those for the primary power levels γ_i, $i = 1,2,\ldots,K$.

5 Simulation Parameters and Settings

To obtain sample Pareto optimal designs using our proposed framework, we selected experimental settings as follows. CIE D65 was chosen (the SPD peak was normalized to 1, which pegs the relative optical power we report to an absolute scale.) as the scene illuminant $l(\lambda)$, which agrees with the Rec. 2020 standard.[1] For the observers, we included the CIE 1931 2° standard observer[13] for gamut coverage computation ($\mathcal{G}_{uv}$) and conventional colorimetric matching in color conversion, and the observers specified in the recently published Observer Function Database,[31] where the 2° CMFs of 151 color-normal observers were individually estimated, for observer variability representation as well as observer metamerism quantification ($\mathcal{M}_O$). For the samples of object reflectances, we selected the Macbeth DC color checker, which is commonly used for camera characterization. All spectral functions were represented using a 1-nm sampling interval over the visible range of 400 to 700 nm. SPDs having a lower sampling rate were upsampled via CIE recommended Sprague interpolation.[32] This relatively fine sampling allows us to represent narrow band primaries with good accuracy while maintaining a coherent framework and reasonable computational cost compared with alternative more sophisticated modeling approaches.[33,34] The feasible range for the peak wavelengths is set between $a_\mu = 400$ nm and $b_\mu = 700$ nm, and spectral widths are constrained to the range from $a_\sigma = 1$ nm to $b_\sigma = 100$ nm. The flare level is set to 0.5%, i.e., $\zeta = 0.005$.

For numerical evaluation of the Pareto front, we used the nondominated sorting genetic algorithm-II (NSGA-II),[35] which is a well-known and widely accepted technique for applications of multiobjective optimization in several different domains. NSGA-II is an evolutionary computation-based iterative algorithm that does not require the computation of gradients and exhibits good convergence to the global Pareto optimal parameter set. We used the implementation of NSGA-II provided in MATLAB® via the function *gamultiobj*. The peak wavelengths μ_1 to μ_K were arranged

in descending order and successive μ_i were constrained to be at least 5 nm apart to avoid numerical instabilities and to speed up the optimization by eliminating redundant representations.

To meaningfully navigate the different options possible through combinations of the three objectives, the four strategies we consider for color conversion, and varying numbers of primaries, we structure our discussion of the results in the following progression. First, we consider the two-objective power ($\mathcal{P}_{\max}$) versus gamut ($\mathcal{G}_{uv}$) Pareto front, because both of these objectives are independent of the color conversion strategy. Next, we consider the two-objective observer metamerism ($\mathcal{M}_O$) versus gamut ($\mathcal{G}_{uv}$) Pareto front and assess the impact of the four alternative color conversion strategies described in Sec. 2.3. Finally, we present the full three-objective Pareto front, restricting our attention to the best performing color conversion strategy with respect to the observer metamerism metric $\mathcal{M}_O$. To manage the computational requirements, the algorithmic parameters for the NSGA-II and the energy budget ranges need to be selected differently for the two and three-objective MOOPs. We used a population size over 1000 for the two-objective optimizations and over 15,000 for the three-objective case, and in both cases, we set the maximum limit on the number of generations to 5000 and used a random initialization. Minor refinements were seeded with the results from past optimization runs. For the two-objective MOOPs, we allow a rather generous energy budget range from $E_B^{(L)} = 20$ to $E_B^{(U)} = 2000$ to allow extremes of the design space to be explored, even though these extremes may be impractical. For three-objective MOOP, the energy budget is limited to a smaller, more relevant region between $E_B^{(L)} = 40$ and $E_B^{(U)} = 180$. The chosen population sizes and parameter ranges ensured that the result of the NSGA-II optimization was not particularly sensitive to initialization provided enough computation time was allowed for the convergence tolerance checks to be satisfied.

6 Results

6.1 *Tradeoff Analysis Between Power ($\mathcal{P}_{\max}$) and Gamut ($\mathcal{G}_{uv}$)*

The optical power ($\mathcal{P}_{\max}$) versus gamut ($\mathcal{G}_{uv}$) Pareto fronts for optimal primary designs for systems with $K = 3$, 4, and 5 primaries are shown in Fig. 2. From the figure, one can appreciate: (1) an increase in the gamut area coverage requires an increase in power, (2) for the same increase in gamut area coverage, a much higher increase in power is required for higher gamut area coverage percentages, and (3) increasing the number of primaries widens the display gamut area only if an adequate level of optical power is available. Specifically, the figure shows that including a fifth primary provides a significant increase in gamut area coverage beyond the optimized four-primary system, only if the total relative power is higher than 10^2 units. Below this threshold for power, the optimized five-primary system provides almost the same gamut area coverage as the optimized four-primary system.

Examination of the parameters for the optimal primary designs on the Pareto front provides additional insights into the nature of the tradeoffs. The spectral width (σ_i) values

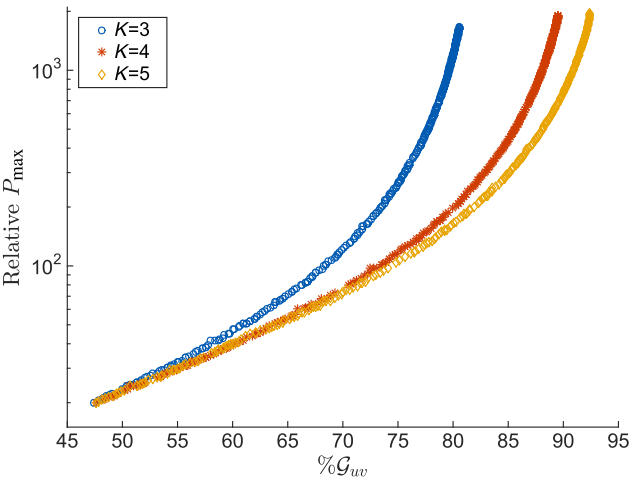

Fig. 2 Pareto fronts characterizing the tradeoff between power consumption and CIE $u'v'$ chromaticity gamut area coverage. The chromaticity gamut area coverage is plotted as a percentage of the total feasible CIE $u'v'$ chromaticity area and denoted by $\%\mathcal{G}_{uv}$. The "curve" formed by the scatter plot of points in each color defines the Pareto optimal front for these two display traits for a given number of primaries (see legend). The points at which the fronts corresponding to different numbers of primaries merge indicate thresholds for optical power (on the y-axis) below which adding primaries beyond the smallest K value among the merged curves is ineffective in expanding the gamut.

are quite small for all designs on the Pareto front irrespective of the number of primaries, implying that optimal designs correspond to narrow band primaries. We therefore focus our attention on the peak wavelength (μ_i) and the primary power (γ_i) parameters and examine their variation along the Pareto fronts. Figure 3 shows the optimal parameters for display systems with $K = 4$ primaries along the $P_{\max}$ versus $\mathcal{G}_{uv}$ Pareto front (arranged in order of increasing gamut area coverage). It can be seen that for the power-gamut Pareto optimal designs, as the gamut area coverage increases, two

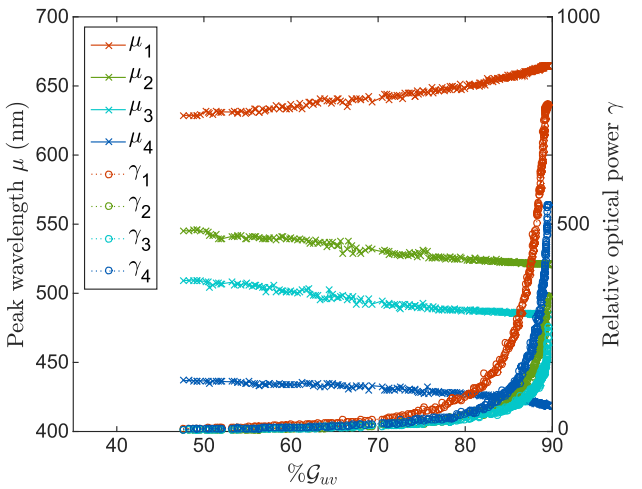

Fig. 3 Distributions of primary parameters for a four-primary display along the Pareto optimal front shown in Fig. 2 (arranged in order of increasing gamut area). For each feasible value of the $\mathcal{G}_{uv}$ along the Pareto front in Fig. 2, there are eight corresponding relevant parameters comprising the peak wavelengths and primary amplitude or relative optical power for the Gaussian spectral profiles. For each primary, the two parameters μ_i and γ_i, corresponding, respectively to peak wavelength and optical power, are shown in identical color and differentiated by different line styles.

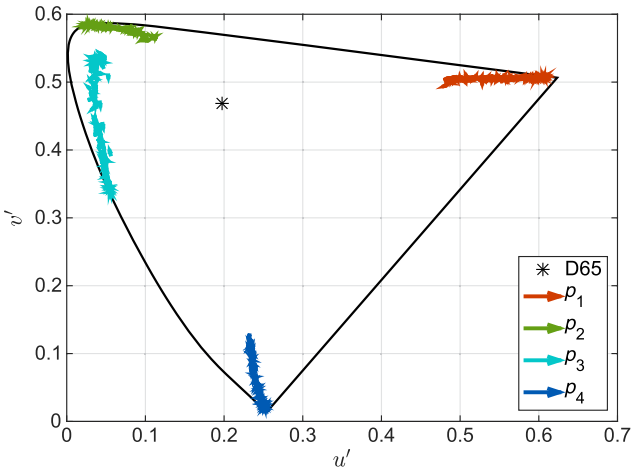

Fig. 4 Channel chromaticity trajectories for a four-primary display along the Pareto optimal front shown in Fig. 2. Each channel chromaticity corresponds to the chromaticity for the SPD resulting from the combination of the corresponding primary with the flare. The trajectories indicate how the channels move toward the spectral locus for enabling larger gamut area coverage.

of the peak wavelengths move toward the extremes of the visible region of spectra while the other two are centered in the middle of the range of visible wavelengths. As one approaches the limiting value of the maximum gamut area coverage, the γ_i's representing the relative power of the primaries increase rapidly. This increase is particularly marked for the two primaries whose peak wavelengths λ_i have values approaching the extreme wavelengths in the visible range. Compared to the other primaries, a higher power is required to counter the impact of the flare when one wishes to push these primaries outward in chromaticity to increase the gamut area coverage. Note that the trend indicates that the "ideal" gamut area coverage would push peak wavelengths to 400 and 700 nm, but that would require a significant amount of primary power γ_i, and thus, such a design would not be practical and is not reached under the power budget constraint imposed. To aid visualization, in Fig. 4, we also show the trajectories for each of the channel chromaticities along the Pareto front for the optimal parameter values plotted in Fig. 3. These trajectories show how, as the power is increased, the channel chromaticities progressively migrate toward the spectrum locus corresponding to locations that yield the optimal gamut area coverage for a four-primary system.

6.2 *Tradeoff Analysis Between Observer Metamerism ($\mathcal{M}_O$) and Gamut ($\mathcal{G}_{uv}$)*

As indicated earlier, for multiprimary displays, the observer metamerism index $\mathcal{M}_O$ depends not only on the choice of primaries but also on the strategy used for color conversion. In particular, the SACM and MOTA strategies are selected with a view to minimizing observer metamerism, directly in the latter case and in the former case, through the correlation between spectral reproduction accuracy and observer metamerism. We consider the two-objective observer metamerism ($\mathcal{M}_O$) versus gamut ($\mathcal{G}_{uv}$) Pareto front, beginning by examining the influence of the alternative strategies for color conversion.

6.2.1 *Comparison between different color conversion strategies*

Figures 5(a)–5(c) show the observer metamerism ($\mathcal{M}_O$) versus gamut ($\mathcal{G}_{uv}$) Pareto fronts for $K = 3$, 4, and 5 primaries, respectively, comparing, in each case the four strategies for color conversion, namely, CMMS, SACM, MOTA, and NSA. The results reflect the expected inherent conflict between observer metamerism and gamut area: irrespective of the color conversion strategy used, reducing observer metamerism penalizes gamut area, whereas increasing gamut area comes at the cost of increasing observer metamerism. The CMMS, SACM, and MOTA color conversion methods, which prioritize colorimetric matching for the standard observer, have significantly lower (better) observer metamerism than the NSA color conversion approach, especially for three- and four-primary displays. This observation reinforces the utility and primacy of the CIE standard observer model, despite the challenges of observer metamerism. For the three-primary display, the CMMS, SACM, and MOTA methods collapse into a single Pareto front because the colorimetric match requirement leaves no additional freedom in the selection of control values (this result also serves as a parity check). For four- and five-primary displays, the MOTA approach has the lowest (best) observer metamerism. For four-primary displays, the observer metamerism of the SACM method is comparable to that of the CMMS; while the SACM strategy does reduce the spectral error (results not shown), the reduction does not translate to a corresponding reduction in the observer metamerism metric. When the number of primaries is increased to 5, however, the benefit of emphasizing spectral accuracy becomes more obvious:

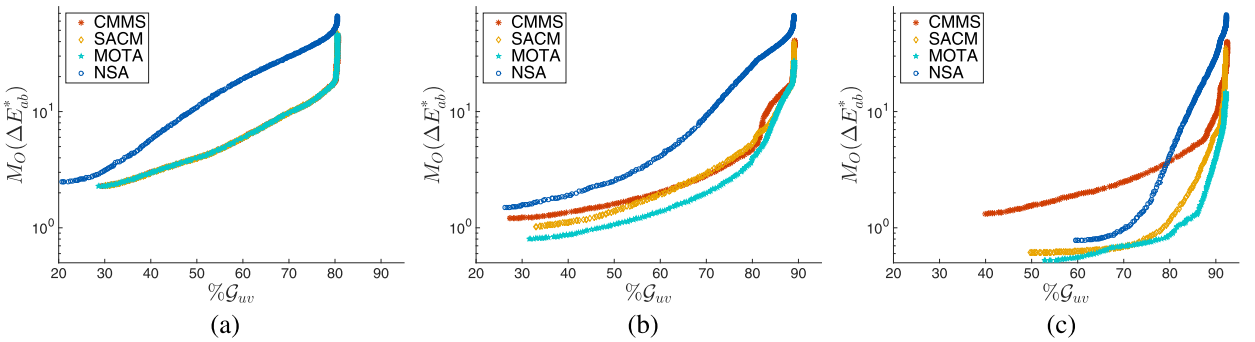

Fig. 5 The Pareto fronts of observer metamerism $\mathcal{M}_O$ versus gamut area coverage $\mathcal{G}_{uv}$ for (a) three-, (b) four-, and (c) five-primary displays, obtained using color conversion using CMMS, SACM, and MOTA, and NSA.

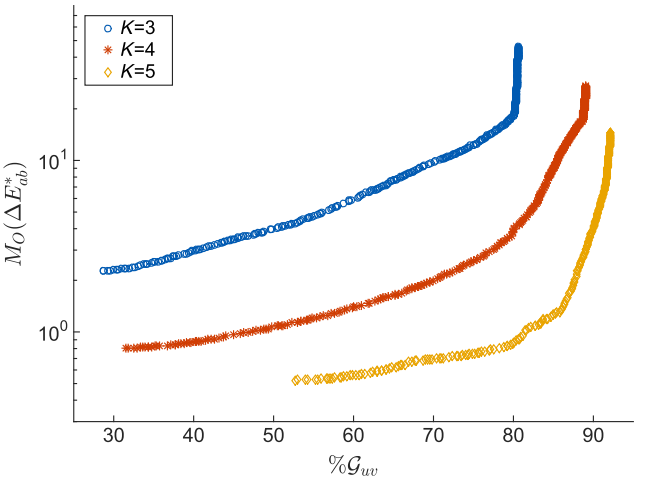

Fig. 6 Pareto fronts characterizing the tradeoff between observer metamerism and CIE $u'v'$ chromaticity gamut area coverage. Note that for designs with fewer than five primaries, there is a strong tradeoff between the two traits: primaries that maximize the gamut area coverage exhibit a high degree of observer metamerism, and vice versa. With increasing number of primaries, the tradeoff between the two traits eases.

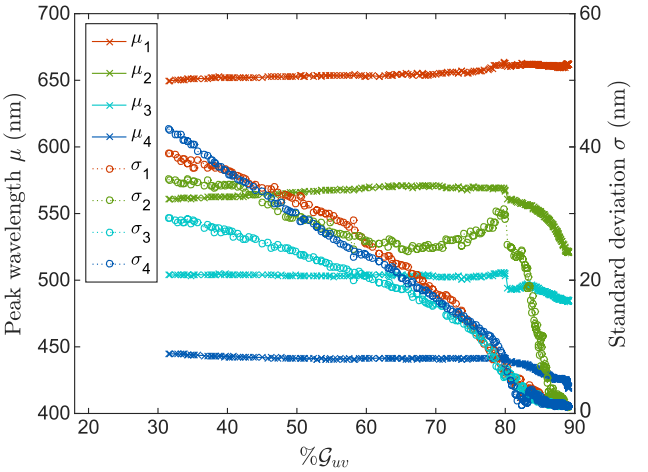

Fig. 7 Parameters for the Pareto optimal four-primary designs in Fig. 6 [for observer metamerism ($\mathcal{M}_O$) versus gamut ($\mathcal{G}_{uv}$), arranged in order of increasing gamut area coverage]. Peak wavelength and standard deviation for a primary are shown in a single color and differentiated by different line styles.

the SACM approach does significantly better than CMMS over almost the entire Pareto front and for gamut area coverage below 78%, even the NSA approach improves over CMMS. Overall, the MOTA approach performs best in that has the lowest observer metamerism among the approaches considered and is therefore used in results presented in subsequent sections.

6.2.2 *Observer metamerism ($\mathcal{M}_O$) versus gamut ($\mathcal{G}_{uv}$) Pareto fronts*

Figure 6 presents the observer metamerism ($\mathcal{M}_O$) versus gamut ($\mathcal{G}_{uv}$) Pareto fronts for $K = 3$, 4, and 5 primaries. Unless explicitly specified otherwise, for these and subsequent results presented in this paper, color conversion is performed using the MOTA approach, which was shown to have the best performance in the preceding section. The results indicate that adding primaries offers a clear advantage for optimizing each of the objectives and for enabling better compromises. For instance, given a design requirement for a specific level of gamut coverage, the display with a larger number of primaries performs better in the minimization of observer metamerism. The Pareto fronts can be helpful to determine the minimum number of primaries required to satisfy requirements for the two objectives. For example, an observer metamerism index under 1 ΔE^*_{ab} with over 70% coverage of the feasible CIE $u'v'$ chromaticity area can only be obtained by using at least $K = 5$ primaries.

Figure 7 shows the parameters for the optimal primary designs along the $\mathcal{M}_O$ versus chromaticity gamut coverage $\mathcal{G}_{uv}$ Pareto front for four-primary designs (arranged in increasing gamut area coverage order). The primary bandwidths σ_i exhibit greater variation along this Pareto front, suggesting that these are the main parameters driving the tradeoffs between the two-objective functions: a larger gamut requires narrow band primaries while lower observer metamerism requires wide band primaries. The peak wavelengths μ_i show some "discontinuous" jumps that appear anomalous at first glance but upon examining the channel chromaticity trajectories in the chromaticity plane (figure not shown) can be seen to correspond to switch between alternative geometric configurations of the primaries (channels) that provide optimal gamut area coverage as $\mathcal{M}_O$ is varied. The μ_i values for maximum gamut area coincide with the result in Fig. 3. Interestingly, for minimum observer metamerism in the three-primary designs, the three peak wavelengths are approximately coincident with the prime wavelengths of 450, 540, and 605 nm,[36] although for the optimal $K = 4$ and 5 primary designs no relation is observed between the optimal primary wavelengths and the prime wavelengths. The parameters γ_i all remain nearly constant across the Pareto front. Higher values of these parameters are desirable for both $\mathcal{M}_O$ minimization and $\mathcal{G}_{uv}$ maximization but their sum is directly subject to the energy budget constraint (E_B) and the results therefore indicate that the Pareto optimal designs maintain the same relative allocation of power among the primaries.

6.3 *Three Objective Pareto Front for Power ($\mathcal{P}_{\max}$), Gamut ($\mathcal{G}_{uv}$), and Observer Metamerism ($\mathcal{M}_O$)*

Next, we consider a comprehensive view of the tradeoffs between the objectives of power ($\mathcal{P}_{\max}$), gamut ($\mathcal{G}_{uv}$), and observer metamerism ($\mathcal{M}_O$) by considering the three-objective Pareto optimal designs. The two-objective Pareto fronts explored in the preceding sections indicate that power represents a common limitation for the optimization of both gamut area and observer metamerism, we focus the exploration of the three-objective Pareto front to the power range between $E_B^{(L)} = 40$ and $E_B^{(U)} = 180$ over which the two other attributes take reasonable values in the two-objective comparisons. Figure 8 shows the $K = 3$, 4, and 5 primary Pareto fronts for the three objectives as a surface (the computed scatter plot is interpolated for display) in the 3-D space determined by the power ($\mathcal{P}_{\max}$), gamut ($\mathcal{G}_{uv}$), and observer metamerism ($\mathcal{M}_O$) axes. As the power $\mathcal{P}_{\max}$ increases, there is Pareto improvement for observer metamerism $\mathcal{M}_O$ and gamut coverage $\mathcal{G}_{uv}$, i.e., either both traits can be improved simultaneously or one can be improved

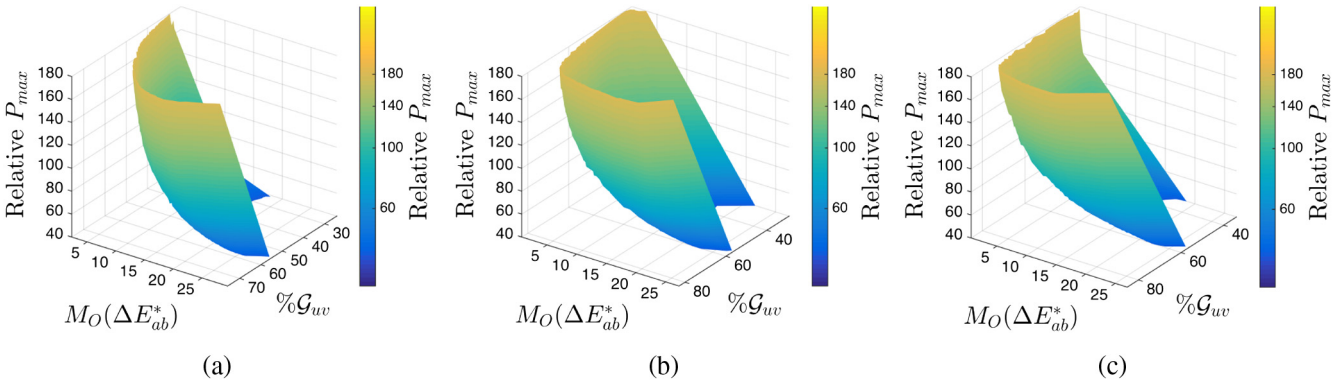

Fig. 8 The Pareto front surface for power ($\mathcal{P}_{\max}$), gamut ($\mathcal{G}_{uv}$), and observer metamerism ($\mathcal{M}_O$), for (a) three-, (b) four-, and (c) five-primary displays. Each power level can be seen as a power budget constraint, and the corresponding slice is 2-D Pareto front shown earlier in Fig. 6.

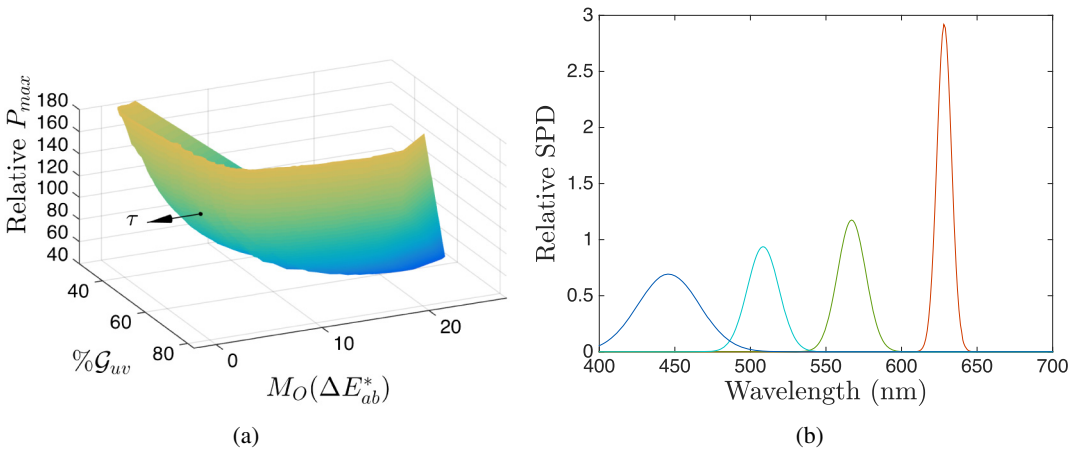

Fig. 9 Example illustrating the relation between the (a) Pareto front and (b) optimal designs obtained by weighted linear combinations of individual metrics for a four-primary design. We consider the design that maximizes the weighted metric $(-1.00\mathcal{P}_{\max} + 0.15\mathcal{G}_{uv} - 55.33\,\mathcal{M}_O)$. The corresponding optimized four-primary design has a chromaticity gamut area $\mathcal{G}_{uv} = 61.1\%$ of the total feasible area, observer metamerism index $\mathcal{M}_O = 2.92\Delta E^*_{ab}$, and maximum optical power $\mathcal{P}_{\max} = 122.3$, which corresponds to the point on the Pareto front in (a) where the weight vector $\boldsymbol{\tau} = [-1.00, 0.15, -55.33]^T$ forms a normal to the Pareto front surface (as shown). The designed primaries are defined by the parameters: peak wavelengths $\mu_i = 628.3$, 567.0, 508.4, and 445.9 nm, standard deviations $\sigma_i = 4.8$, 9.3, 10.4, and 20.4 nm, and power amplitudes $\gamma_i = 35.2$, 27.3, 24.4, 35.3, respectively.

without requiring a compromise in the other. The slopes of the Pareto surfaces with respect to $\mathcal{P}_{\max}$ are steeper for larger K, which once again highlight the mitigation in the tradeoff when more primaries are available.

Note that the two-objective Pareto fronts can be obtained from the three-objective Pareto front by projecting the 3-D Pareto surface onto the corresponding two-objective plane by dropping the third objective and then eliminating dominated points, i.e., points for which at least one of the attributes is improved without a compromise of the other. Specifically, in addition to the two-objective Pareto fronts shown in prior subsections, the remaining two-objective tradeoff between power ($\mathcal{P}_{\max}$) versus observer metamerism ($\mathcal{M}_O$) can also be seen from the three-objective Pareto front as its projection on the $\mathcal{P}_{\max} - \mathcal{M}_O$ plane followed by removal of dominated points.

While the two-objective Pareto fronts and their Pareto optimal solutions are helpful for analyzing the interrelation between pairs of parameters, the three-objective Pareto fronts offer more complete view comprehending all design objectives and are therefore more useful in making final design choices for primaries. In particular, all solutions obtained by optimizing a single metric formed by a weighted linear combination of the individual attribute metrics of power ($\mathcal{P}_{\max}$), gamut ($\mathcal{G}_{uv}$), and observer metamerism ($\mathcal{M}_O$) lie on the Pareto front. Specifically, the optimal solution for maximizing $(-\tau_p\mathcal{P}_{\max} + \tau_g\mathcal{G}_{uv} - \tau_m\mathcal{M}_O)$, $(0 \le \tau_p, \tau_g, \tau_m)$, is the point on the Pareto surface defined by the value of for which the plane $(-\tau_p\mathcal{P}_{\max} + \tau_g\mathcal{G}_{uv} - \tau_m\mathcal{M}_O) = \psi$ is tangential to the Pareto surface;[30] the vector of weights $\boldsymbol{\tau} = [-\tau_p, \tau_g, -\tau_m]^T$ then defines the normal for the tangent plane. Figure 9 shows this fact using a specific four-primary design example (see caption for detail). Solutions for such a weighted optimization using any choice of weights can therefore be determined from the 3-D Pareto surface. The converse, however, does not hold. Because there exist non-convex regions on the Pareto fronts (see the $K = 5$ case in Fig. 6), not all points on the Pareto front correspond to a solution of a weighted optimization.[30]

7 Discussion

Several observations are worth noting regarding the proposed MOOP framework for display primary design and the results we presented. First, even though the level of flare is quite low (at 0.5%), it is critical that flare be considered in the primary design process. As already noted, in the absence of flare, a very small amount of energy allocated to a primary placed on the spectrum locus can cause a significant increase in the chromaticity gamut coverage resulting in numerical instability for the proposed optimization (an analogous problem also plagues CIELAB[37]).

Second, it is important to note that the color conversion approach strongly influences the observer metamerism metric for multiprimary displays. The CMMS approach, which only takes into account colorimetric matching, performs quite poorly for $K = 4$ and 5 primaries, which represent situations most likely to be considered in current practical designs. Interestingly, the NSA approach that focuses only on spectral reproduction performs consistently worse than CMMS for $K = 3$ and 4 primaries and also for $K = 5$ primaries for gamut coverage over 78% of the feasible CIE $u'v'$ chromaticity area. Thus, aiming for spectral reproduction appears to an inappropriate design goal unless the number of primaries is significantly larger. The SACM approach that minimizes spectral error while ensuring a colorimetric match performs reasonably but is outmatched by the MOTA approach that focuses more directly on observer metamerism. Particularly, for $K = 4$ primaries, the MOTA color conversion approach offers a significant gain over SACM. This highlights the fact that although the spectral error correlates with the observer metamerism, the correlation is far from perfect for displays with 5 or less primaries. The SACM and MOTA color conversion approaches require that spectral information be available for images that the display seeks to reproduce. The lack of such information in current color capture and color management workflows poses a challenge for the adoption of these approaches. However, we anticipate that technological advances and new emerging applications, such as augmented reality, will favor the use of spectral approaches for better agreement/consistency between the real-world and display rendered imagery. Note that environments where a direct real-world view is combined with a displayed image also provides better justification for our observer metamerism metric.

In our investigation, we also examined the potential impact of using different color conversion strategies for the display design process and for the display use after the design has been completed. This examination was motivated by the idea that computational simplicity may motivate a simpler color conversion strategy (e.g., NSA or CMMS) in the design stage and a more sophisticated strategy (e.g., SACM or MOTA) may be used in practice, once a specific design has been chosen. Figure 10 summarizes the results from this exploration. The results demonstrate that while improvements can be obtained, in some situations, using a more sophisticated strategy for color conversion after designing using a simpler strategy (e.g., NSA-MOTA), these designs invariably do not offer competitive performance (for observer metamerism) compared with using the best performing MOTA method in both the design and practice stages. These results also highlight that prior approaches[8,12] that used simplified color conversion approaches for the design stage cause significant performance compromises.

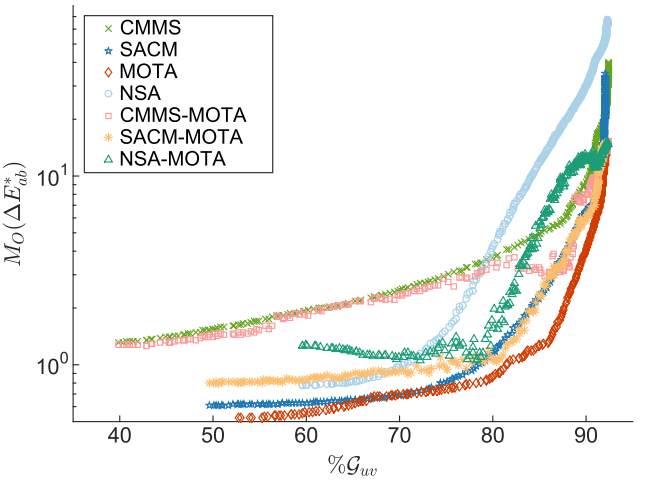

Fig. 10 Observer metamerism $\mathcal{M}_O$ versus chromaticity gamut coverage $\mathcal{G}_{uv}$ for a five-primary display using alternative primary designs from Fig. 5(c) in combination with different color conversion methods. Legends in the format "A-B" indicate the performance of Pareto optimal designs obtained using method "A" for color conversion in the design stage and method "B" in actual rendering. Legends in the format "A" refer to the situation where the method "A" is used in both stages.

We note that while there is a tradeoff between observer metamerism and the gamut coverage, these two attributes are not completely opposed to each other. Specifically, for colors on the spectrum locus, only spectral (nonmetameric) matches are feasible and therefore inclusion in the gamut coincides with minimization of observer metamerism (a zero value for our observer metamerism metric). In practical applications, reflective colors on the spectrum locus are not meaningful. However, by extrapolation, one can also expect that for other highly saturated colors, inclusion within the gamut will correlate with reduction of observer metamerism. The proposed framework does not preclude such correlation. However, the exact Pareto fronts and optimal parameter values will depend on the dataset of reflectances used for assessment of observer metamerism and on the set of observer CMFs. In the results presented in this paper, we formulate our observer metamerism metric using the Macbeth DC color patches that are designed for calibration of color cameras and representative of the range of commonly encountered colors.

In the context of alternative RGB color encoding standards for video,[1,38] recent work[39,40] has analyzed the relation between chromaticity gamut area in various spaces and the corresponding gamut volume in a perceptual space. Specifically, the work considered the percentage of the 3-D Rec. 2020[1] encoding gamut volume in CIELAB or CIELUV spaces that is covered by a set of three primaries that also include the Rec. 709[38] chromaticity gamut and demonstrated that this percentage exhibits a better monotonic relation with the CIE xy chromaticity gamut area as compared with the CIE $u'v'$ chromaticity gamut area. Although our work was not specifically motivated by coverage of these standard encodings, we note that our framework can also be readily utilized alternatively with the CIE xy chromaticity gamut area. Data included with the implementation that we provide for our framework[41] also include

results for the multiobjective optimization computed using the CIE *xy* chromaticity gamut area, although in the interest of brevity, these are not included within this article.

Finally, we note that although we considered the color metrics of key importance in the design of color display primaries, often additional objectives and tradeoffs come into play in display design. Specifically, for several common designs such as OLED and LCD displays, the primaries must share spatial area available for a display pixel. Thus, the addition of primaries causes a tradeoff in the spatial resolution of the display. While an exploration of this aspect is beyond the scope of the current paper, with availability of additional computational power and models and spatiospectral datasets one could also incorporate additional metrics in the proposed framework to account for such a tradeoff. The software implementation we provide[41] should also facilitate such alternative explorations.

8 Conclusion

This paper proposes a multiobjective optimization framework for designing display primary spectra for three- and multiprimary displays and presents and analyzes designs obtained in the proposed framework for optimizing three key display traits: power consumption, gamut coverage, and observer metamerism. The results highlight the tradeoffs between the desired objectives of minimizing power consumption, maximizing gamut coverage, and minimizing observer metamerism. Compared to traditional three-primary displays, multiprimary systems have a significant advantage for easing the tradeoff among different objectives, although advantages of using more primaries are only realized once available power exceeds a minimal threshold. The method used for color conversion for multiprimary displays has a significant impact on observer metamerism. For the three-, four-, and five-primary display primary designs investigated in this paper, a color conversion strategy that minimizes the total squared tristimulus error over the observer population offers a significant advantage over alternatives that minimize spectral error, either directly (NSA) or under a colorimetric matching constraint (SACM).

The MATLAB™ source code for our implementation and the Pareto optimal designs featured in the results are available.[41]

Appendix A: CMMS Color Conversion Approach

The CMMS method partitions the gamut into quadrangle pyramids based on the gamut facets and computes control values for each in-gamut color using the pyramid in which the color lies.

A.1 Gamut Decomposition by Quadrangle Pyramids

The display gamut in CIEXYZ space is a special type of polyhedron known as zonohedron.[42,43] The gamut boundary is composed of $K(K-1)$ gamut facets; each facet is a parallelogram spanned by a pair of primaries, as can be seen in Fig. 11. Zonohedrons have central symmetry,[44] which implies that every pair of primaries $\mathbf{p}_k$, $\mathbf{p}_l$, and $1 \le k < l \le K$ spans a pair of opposite and parallel gamut facets $\mathcal{S}^{klm}$, mathematically represented as

$$\mathcal{S}^{klm} = \mathbf{p}_0 + \mathbf{q}^{klm} + \{\beta\mathbf{p}_k + \xi\mathbf{p}_l | 0 \le \beta, \xi \le 1\}, \tag{17}$$

where the display black $\mathbf{p}_0$ represents the origin of the gamut, the index $m = 1{,}2$ differentiates between the two parallel facets, and the vector $\mathbf{q}^{klm}$ is the origin of the facet $\mathcal{S}^{klm}$ relative to the display black, and can be computed as a binary combination of primaries other than $\mathbf{p}_k$ and $\mathbf{p}_l$ as

$$\begin{aligned}\mathbf{q}^{klm} &= \sum_{i=1}^{K} \delta_i^{klm}\mathbf{p}_i \\ &= [\mathbf{p}_1, \mathbf{p}_2, \ldots, \mathbf{p}_K]\boldsymbol{\delta}^{klm},\end{aligned} \tag{18}$$

where $\boldsymbol{\delta}^{klm} = [\delta_1^{klm}, \ldots, \delta_K^{klm}]$ is the primary indicator vector for facet origin $\mathbf{q}^{klm}$, where δ_i^{klm} is a binary value indicating whether the $\mathbf{p}_i$ contributes to the origin of the m'th facet or not. Specifically, we define

$$\delta_i^{klm} = \begin{cases} 1, & \text{if } m = 2 \quad \text{and} \quad \mathbf{p}_i^T(\mathbf{p}_k \otimes \mathbf{p}_l) < 0 \\ 1, & \text{if } m = 1 \quad \text{and} \quad \mathbf{p}_i^T(\mathbf{p}_k \otimes \mathbf{p}_l) > 0 \\ 0, & \text{otherwise,} \end{cases} \tag{19}$$

where the operator $\otimes$ represents the vector cross product.

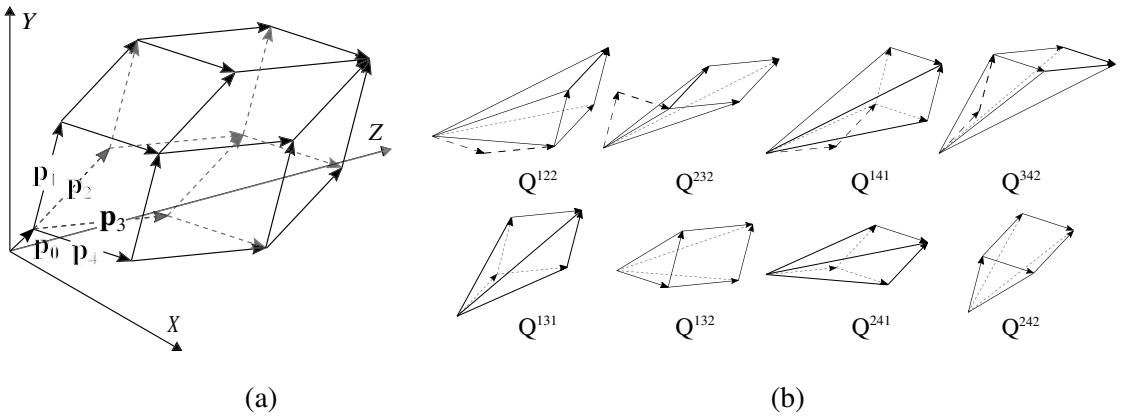

Fig. 11 (a) A $K = 4$ primary display gamut in CIE XYZ space and (b) its quadrangle pyramid decomposition for the CMMS algorithm. Facets of the gamut are comprised of pairs of two opposing and parallel parallelograms spanned by a pair of primaries. Every pair of primaries $\mathbf{p}_k$ and $\mathbf{p}_l$, $1 \le k < l \le K$, spans two distinct parallel facets with origins (relative to $\mathbf{p}_0$) $\mathbf{q}^{kl1}$ and $\mathbf{q}^{kl2}$ that correspond to binary combinations of the remaining primaries. Facets whose origin is not the display black, $\mathbf{q}^{klm} \neq \mathbf{0}$ define a pyramid Q^{klm}. All pyramids defined in this way are nonoverlapping and partition the gamut. The dashed vectors in each pyramid show how primaries are combined to obtain the facet origins.

From the definitions in Eq. (19), it directly follows that $\delta_k^{klm} = \delta_l^{klm} = 0$, and thus, the primaries spanning the facet do not contribute to the origin. Moreover, if three distinct primaries are always noncoplanar, we can conclude from Eq. (19) that every primary not spanning the facet contributes to the origin of one and only one of the two parallel facets. Note that each facet $\mathcal{S}^{\mathrm{klm}}$ for which $\mathbf{q}^{klm} \neq \mathbf{0}$, or equivalently $\boldsymbol{\delta}^{klm} \neq \mathbf{0}$, can serve as the base of a quadrangle pyramid Q^{klm} whose apex is located at the display black $\mathbf{p}_0$. As Fig. 11(b) shows, these pyramids are nonoverlapping and form a decomposition of the display gamut. Observe that, in the gamut example shown in Fig. 11(a), among the parallel facets $\mathcal{S}^{121}$ and $\mathcal{S}^{122}$, the former has the origin at the display black, hence it does not define a pyramid and there is no pyramid Q^{121}, whereas the facet $\mathcal{S}^{122}$ is the base for the pyramid Q^{122} in the gamut decomposition.

A.2 Control Value Computation for Colors Within Each Pyramid

Consider now a surface $\mathcal{S}^{klm}$ for which $\boldsymbol{\delta}^{klm} \neq \mathbf{0}$, and its associated pyramid Q^{klm} shown in Fig. 12. Any color tristimulus $\mathbf{c}$ inside this pyramid can be uniquely expressed in terms of the oblique system of coordinates defined by $\mathbf{q}^{klm}$, $\mathbf{p}_k$, and $\mathbf{p}_l$, as the combination

$$\mathbf{c} = \mathbf{p}_0 + \nu(\mathbf{q}^{klm} + \beta\mathbf{p}_k + \xi\mathbf{p}_l), \tag{20}$$

where colors within the pyramid have a coordinate representation that satisfies the constraints $0 \leq \nu, \beta, \xi \leq 1$. To compute ν, β, and ξ, Eq. (20) can be rearranged as

$$\mathbf{c} = \mathbf{p}_0 + \mathbf{M}^{klm}\mathbf{v}, \tag{21}$$

where $\mathbf{M}^{klm} = [\mathbf{q}^{klm}, \mathbf{p}_k, \mathbf{p}_l]$ is the matrix associated with the pyramid Q^{klm} and the vector $\mathbf{v} = [\nu, \nu\beta, \nu\xi]^T$ expresses color in terms of the system of oblique vector coordinates defined by the basis vectors $\mathbf{q}^{klm}$, $\mathbf{p}_k$, and $\mathbf{p}_l$, in that order. Since $\boldsymbol{\delta}^{klm} \neq \mathbf{0}$, hence $\mathbf{q}^{klm} \neq \mathbf{0}$, and given that no three primaries are coplanar, the matrix $\mathbf{M}^{klm}$ is nonsingular, thus the vector $\mathbf{v}$ can be obtained as

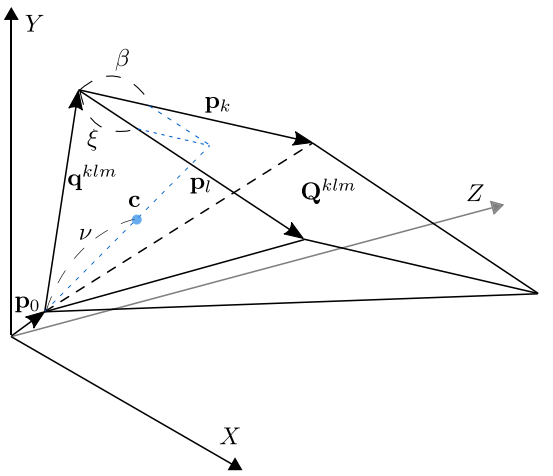

Fig. 12 Quadrangle pyramid Q^{klm} whose base is the gamut facet spanned by primaries $\mathbf{p}_k$ and $\mathbf{p}_l$ and origin $\mathbf{q}^{klm}$ relative to the display black $\mathbf{p}_0$. Every color $\mathbf{c}$ within the pyramid can be expressed as the linear combination $\mathbf{c} = \mathbf{p}_0 + \nu(\mathbf{q}^{klm} + \beta\mathbf{p}_k + \xi\mathbf{p}_l)$, $0 \leq \nu, \beta, \xi \leq 1$.

$$\mathbf{v} = (\mathbf{M}^{klm})^{-1}(\mathbf{c} - \mathbf{p}_0). \tag{22}$$

From Eq. (20), the color tristimulus $\mathbf{c}$ can be expressed as

$$\mathbf{c} = \mathbf{p}_0 + \sum_{\substack{i=1 \\ i \neq k, i \neq l}}^{K} \nu\delta_i^{klm}\mathbf{p}_i + \nu\beta\mathbf{p}_k + \nu\xi\mathbf{p}_l \tag{23}$$

$$= \mathbf{p}_0 + \mathbf{P}\boldsymbol{\alpha}, \tag{24}$$

where $\boldsymbol{\alpha} = [\alpha_1, \ldots, \alpha_K]^T$ is the control vector for the color tristimulus $\mathbf{c}$ in pyramid Q^{klm} computed as

$$\alpha_i = \begin{cases} \nu\beta, & \text{for } i = k, \\ \nu\xi, & \text{for } i = l, \\ \nu\delta_i^{klm}, & \text{otherwise.} \end{cases} \tag{25}$$

Thus, finding the representation of a color tristimulus $\mathbf{c}$ in terms of the oblique coordinate system of pyramid Q^{klm} defines feasible control vector for reproducing the color tristimulus $\mathbf{c}$ on the display. Note also that, conversely, if a color tristimulus $\mathbf{c}$ can be represented as in Eq. (23) while meeting the constraints $0 \leq \nu, \beta, \xi \leq 1$, the color lies inside the pyramid Q^{klm} and therefore inside the gamut. Colors inside the gamut can therefore also be identified by determining if they lie in any of the pyramids Q^{klm} in the quadrangle pyramid gamut decomposition.

A.3 CMMS Algorithm

Based on the preceding description, the CMMS approach for display color conversion can now be summarized as Algorithms 1 and 2. First, Algorithm 1 computes the matrices $\mathbf{M}^{klm}$ and the primary indicator vectors $\boldsymbol{\delta}^{klm}$ for each of the pyramids Q^{klm} in the quadrangle pyramid gamut decomposition. Note that these computations need to be performed only once, and for each primary configuration and these values [and in fact the inverse $(\mathbf{M}^{klm})^{-1}$] can be precomputed and stored for use in Algorithm 2 for all the CMMS color conversions for the primary configuration. Algorithm 2 performs the actual CMMS color conversion using the matrices $\mathbf{M}^{klm}$ and the primary indicator vectors $\boldsymbol{\delta}^{klm}$ provided by Algorithm 1. An indicator variable χ_G output by the algorithm also indicates whether the requested target color $\mathbf{c}$ lies inside or outside the display gamut by values of 1 and 0, respectively. Additionally, the algorithm also outputs another indicator variable χ that indicates, using the same binary value convention, whether the color lies inside one of the cones formed by moving the base of the quadrangle pyramid in the decomposition to an infinite distance from the apex. Specifically, the pyramidal cone corresponding to Q^{klm} is defined by the set of points represented as Eq. (23), where $0 \leq \beta, \xi \leq 1$ and $0 \leq \nu$. (Note the upper bound constraint on ν is dropped for obtaining the cone.) When the color lies inside one of the pyramidal cones, the corresponding representation is returned as the output control vector by Algorithm 2. The auxiliary information is useful for the gamut mapping approach utilized in this paper.

Algorithm 1 CMMS gamut decomposition into quadrangle pyramids.

Input: $\mathbf{P} = [\mathbf{p}_1, \ldots, \mathbf{p}_K]$: $3 \times K$ matrix of primary tristimuli

Output: Matrices $\mathbf{M}^{klm}$, with $1 \le k$, $l \le K$ and $m = 1, 2$ and,

$\boldsymbol{\delta}^{klm} = [\delta_i^{klm}, \ldots, \delta_K^{klm}]$, primary indicator vector for facet origins:

δ_i^{klm} indicates if $\mathbf{p}_i$ contributes to facet origin $\mathbf{q}^{klm}$.

1 **forall** *pairs of primaries* $\mathbf{p}_k$ *and* $\mathbf{p}_l$ $(1 \le k < l \le K)$ **do**

2 $\boldsymbol{\delta}^{kl1}, \boldsymbol{\delta}^{kl2} \leftarrow \mathbf{0}$;

3 **forall** *primaries* $\mathbf{p}_i$, *with* $1 \le i \le K$ **do**

4 **if** $\mathbf{p}_i^T(\mathbf{p}_k \otimes \mathbf{p}_l) > 0$ **then**

5 $\delta_i^{kl1} \leftarrow 1$;

6 **else**

7 $\delta_i^{kl2} \leftarrow 1$;

8 **end**

9 **end**

10 **forall** $m = 1, 2$ **do**

11 $\mathbf{q}^{klm} \leftarrow \mathbf{P}\boldsymbol{\delta}^{klm}$ /* facet origin relative to black */

12 $\mathbf{M}^{klm} \leftarrow [\mathbf{q}^{klm}, \mathbf{p}_k, \mathbf{p}_l]$;

13 **end**

14 **end**

Appendix B: Gamut Mapping

We implemented a two-stage gamut mapping strategy that is simple, yet also approximately hue preserving, which is a trait commonly desired in gamut mapping.[24,25] A given color (tristimulus) $\mathbf{c}$ is first mapped to $\tilde{\mathbf{c}}$, a color with same luminance and $(u'v')$ hue, but whose chromaticity is located inside the display's $u'v'$ chromaticity gamut. Next, the color $\tilde{\mathbf{c}}$ is mapped to a color $\hat{\mathbf{c}}$ inside the display tristimulus gamut, (approximately) preserving chromaticity and adjusting the luminance, if required. Details of the two steps are presented next. Throughout our description, we invariably use the term hue to mean the hue-correlate in CIE $u'v'$ chromaticity diagram (exceptions are apparent based on context).

B.1 Hue-Preserving Chromaticity Mapping

The first stage maps the specified target color $\mathbf{c}$ to a color $\tilde{\mathbf{c}}$ that has identical luminance and hue but is assured to be in the display chromaticity gamut. Specifically, if the chromaticity coordinates $(u_\mathbf{c}, v_\mathbf{c})$ of $\mathbf{c}$ are already inside the (approximate) chromaticity gamut of the display, $\tilde{\mathbf{c}}$ is set identical to $\mathbf{c}$, otherwise, the CIE $u'v'$ chromaticities $(u_\mathbf{c}, v_\mathbf{c})$ of the target color are mapped onto the boundary of the display's (approximate) chromaticity gamut in a hue-preserving manner as shown in Fig. 13. Chromaticities $(\tilde{u}_\mathbf{c}, \tilde{v}_\mathbf{c})$ are obtained as the intersection of the gamut polygon approximation (magenta dashed lines) with the constant-hue line-segment joining the chromaticity coordinates $(u_\mathbf{c}, v_\mathbf{c})$ of the target color $\mathbf{c}$ with the chromaticity coordinates $(u_\mathbf{w}, v_\mathbf{w})$ of the reference white $\mathbf{w}$. The color tristimulus $\tilde{\mathbf{c}}$ is then

Algorithm 2 CMMS control value computation.

Input: $\mathbf{c}$: target color tristimulus,

$\mathbf{p}_0$: display black tristimulus,

$\mathbf{M}^{klm}$: Matrices associated with pyramids from gamut decomposition and

$\boldsymbol{\delta}^{klm}$: Indicator vector for the facets origins (Algorithm 1).

Output: $\boldsymbol{\alpha} = [\alpha_1, \ldots, \alpha_K]^T$, display control vector for color $\mathbf{c}$.

χ, indicates whether $\mathbf{c}$ is inside any pyramidal cone, and

χ_G, indicates whether $\mathbf{c}$ is inside display gamut

1 **forall** pyramid matrices $\mathbf{M}^{klm}$ such that $\boldsymbol{\delta}^{klm} \neq \mathbf{0}$ **do**

2 $\boldsymbol{\alpha} \leftarrow \mathbf{0}$;

3 $\chi, \chi_G \leftarrow 0$;

/* Compute tentative control values for matrix $\mathbf{M}^{klm}$ */

4 $[\nu, \nu\beta, \nu\xi]^T \leftarrow [\mathbf{M}^{klm}]^{-1}(\mathbf{c} - \mathbf{p}_0)$;

5 **if** $0 \le \nu\beta \le \nu$, $0 \le \nu\xi \le \nu$, and $0 \le \nu$ **then**

/* $\mathbf{c}$ is in cone for Q^{klm}, return corresponding $\boldsymbol{\alpha}$ */

6 $\alpha_k \leftarrow \nu\beta$;

7 $\alpha_l \leftarrow \nu\xi$;

8 **forall** $i = 1,2, \ldots, K$, $i \neq k, l$ **do**

9 $\alpha_i \leftarrow \nu\delta_i^{klm}$;

10 **end**

11 $\chi \leftarrow 1$/* In pyramidal cone */

12 **if** $\nu \le 1$ **then**

13 $\chi_G \leftarrow 1$/* In gamut */

14 **end**

15 **break**;

16 **end**

17 **end**

/* If $\chi = 1$, $\boldsymbol{\alpha}$ is the control representation for $\mathbf{c}$ in the pyramidal cone that contains it. If additionally, $\chi_G = 1$, $\mathbf{c}$ is also in the gamut. */

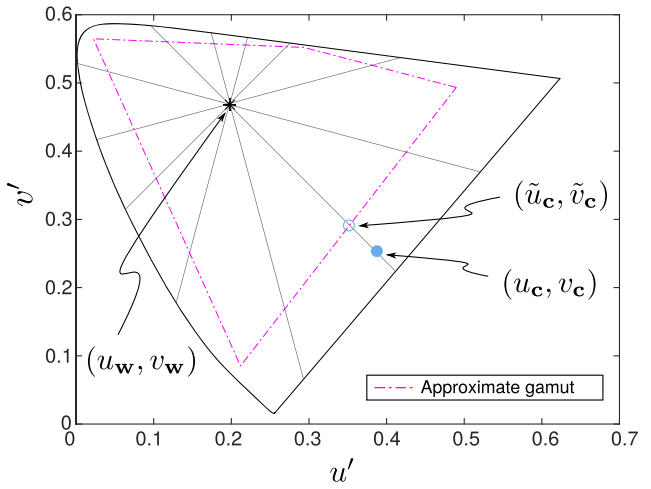

Fig. 13 The first stage of the gamut mapping process, namely, hue-preserving chromaticity mapping, illustrated on the CIE $u'v'$ chromaticity diagram for target color chromaticities $(u_{\mathbf{c}}, v_{\mathbf{c}})$ that are outside the display's chromaticity gamut. The chromaticities $(u_{\mathbf{c}}, v_{\mathbf{c}})$ are mapped to the chromaticities $(\tilde{u}_{\mathbf{c}}, \tilde{v}_{\mathbf{c}})$ obtained as the intersection of the gamut polygon approximation (magenta dashed lines) with the constant-hue line-segment joining the chromaticity coordinates $(u_{\mathbf{c}}, v_{\mathbf{c}})$ with the chromaticity coordinates $(u_{\mathbf{w}}, v_{\mathbf{w}})$ of the reference white **w**.

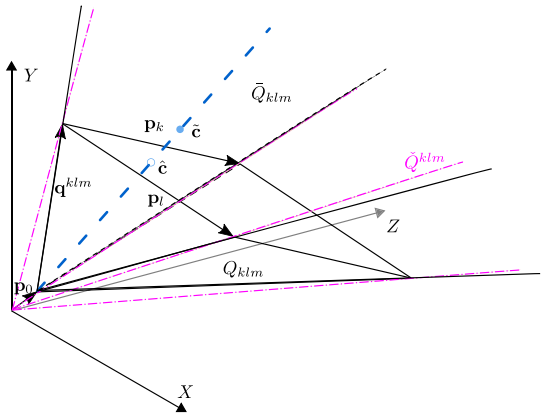

Fig. 14 The second stage of the gamut mapping illustrated for colors in the chromaticity cone $\bar{Q}_{klm}$ delineated by magenta lines corresponding to the range of the display chromaticity gamut spanned by the quadrangle pyramid Q^{klm} (delineated by black lines including the base spanned by primaries $\mathbf{p}_k$ and $\mathbf{p}_l$). Colors within Q^{klm} are unchanged. The relatively small region of colors $\tilde{\mathbf{c}}$ in that are closer to the display black $\mathbf{p}_0$ than the point on the base of Q^{klm} with identical chromaticity (the lower part of the magenta delineated cone $\breve{Q}^{klm}$ not included in Q^{klm}) are mapped to the display black $\mathbf{p}_0$. A color such as the one labeled $\tilde{\mathbf{c}}$ that is further from the display black $\mathbf{p}_0$ than the point on the base of Q^{klm} with identical chromaticity (the upper part of the magenta delineated cone Q_{klm} not included in Q^{klm}) is mapped, as shown, to the point $\hat{\mathbf{c}}$ where the line segment joining $\tilde{\mathbf{c}}$ to the display black chromaticity $\mathbf{p}_0$ intersects with the base of the quadrangle pyramid Q^{klm}. The process is approximately (exactly) chromaticity preserving when the level of flare is low (zero). The mapping is computed using Algorithm 2 as described in the text.

obtained by setting the luminance identical to **c** and CIE $u'v'$ chromaticities $(\tilde{u}_{\mathbf{c}}, \tilde{v}_{\mathbf{c}})$. This stage uses the approximate chromaticity gamut formed by the convex polygon defined by the channel chromaticities as the vertices. As noted in Sec. 3.1.1, the actual display chromaticity gamut is slightly larger. Hence, the approximation is conservative and ensures that mapped colors are inside the display's actual chromaticity gamut.

B.2 Luminance Mapping

While the chromaticity of the color $\tilde{\mathbf{c}}$ obtained from the first stage of the gamut mapping is inside the display's chromaticity gamut, the color $\tilde{\mathbf{c}}$ is not assured to lie inside the 3-D tristimulus gamut for the display. To complete the gamut mapping process, the second stage maps the color $\tilde{\mathbf{c}}$ to a color $\hat{\mathbf{c}}$ in the 3-D display gamut by keeping the chromaticity (approximately) unchanged and adjusting the luminance, if required. Specifically, if $\tilde{\mathbf{c}}$ is already inside the 3-D tristimulus gamut, $\hat{\mathbf{c}}$ is set identical to $\tilde{\mathbf{c}}$, otherwise the luminance of $\hat{\mathbf{c}}$ is scaled while keeping the chromaticity (approximately) unchanged to obtain $\hat{\mathbf{c}}$ in the 3-D tristimulus display gamut. This luminance scaling process exploits the geometrical properties of the gamut decomposition and color conversion introduced for the CMMS method in Appendix A. Consider a specific quadrangle pyramid Q^{klm} and consider the corresponding quadrangle cone $\bar{Q}^{klm}$ obtained by moving the base to an infinite distance from the apex $\mathbf{p}_0$ as shown in Fig. 14. Mathematically,

$$\bar{Q}^{klm} = \{\mathbf{p}_0 + \nu(\mathbf{q}^{klm} + \beta\mathbf{p}_k + \xi\mathbf{p}_l) | 0 \le \beta, \xi \le 1, 0 \le \nu\}, \tag{26}$$

where compared with the corresponding quadrangle pyramid Q^{klm}, the upper bound constraint $\nu \le 1$ has been dropped.

The quadrangle pyramids Q^{klm} from the CMMS color conversion process provide a partitioning of the display chromaticity gamut. We therefore use the individual quadrangle pyramids and cones as the basis for the second stage of the gamut mapping process mapping colors $\tilde{\mathbf{c}}$ within the quadrangle cone $\bar{Q}^{klm}$ corresponding to the quadrangle pyramid Q^{klm} in which the chromaticity of $\tilde{\mathbf{c}}$ lies. The process is shown in Fig. 14 for a single quadrangle pyramid Q^{klm} and corresponding cone $\bar{Q}^{klm}$. The magenta dashed lines in the figure define an additional quadrangle cone $\breve{Q}^{klm}$ corresponding to the cone of colors whose chromaticity lies in the chromaticity gamut of the quadrangle pyramid Q^{klm}. The figure describes the second stage of the gamut mapping process for the colors in the cone $\breve{Q}^{klm}$. As already indicated, if $\tilde{\mathbf{c}}$ lies in Q^{klm}, $\hat{\mathbf{c}}$ is set identical to $\tilde{\mathbf{c}}$. The figure illustrates that when $\tilde{\mathbf{c}}$ does not lie in Q^{klm}, there are two possibilities. If $\tilde{\mathbf{c}}$ is closer to the display black $\mathbf{p}_0$ than the point on the base of Q^{klm} with identical chromaticity (the lower part of the magenta delineated cone $\breve{Q}^{klm}$ not included in Q^{klm}), it is simply mapped to the display black, viz., $\hat{\mathbf{c}}$ is set to $\mathbf{p}_0$, or equivalently the display control values are set to $\mathbf{0}$. Because the level of flare is quite low, this region on the "lower side" is actually quite small in practice (despite the exaggerated size in the figure) and therefore did not warrant special consideration. If, on the other hand, $\tilde{\mathbf{c}}$ is further from the display black $\mathbf{p}_0$ than the point on the base of Q^{klm} with identical chromaticity (the upper part of the magenta delineated cone $\breve{Q}^{klm}$ not included in Q^{klm}), it is mapped along an approximate isochromaticity line to the base of the pyramid Q^{klm} as shown in Fig. 14. From Fig. 14, we can see that in this situation, the color $\tilde{\mathbf{c}}$ lies

Algorithm 3 Approximate hue-preserving gamut mapping based on CMMS.

Input: $\mathbf{c}$: target color tristimulus,

$\mathbf{P} = [\mathbf{p}_1, \ldots, \mathbf{p}_K]$: $3 \times K$ matrix of primary tristimuli,

$\mathbf{p}_0$: tristimulus of the display black,

$\mathbf{w}$: tristimulus of the white reference,

$\mathbf{M}^{klm}$: Matrices associated to pyramids from gamut decomposition and

$\boldsymbol{\delta}^{klm}$: Indicator vector for the facets origins (Algorithm 1)

Output: $\hat{\mathbf{c}}$: mapped color inside display gamut, and

$\hat{\boldsymbol{\alpha}} = [\hat{\alpha}_1, \ldots, \hat{\alpha}_K]^T$: corresponding vector of control values.

/* Stage I: Hue-preserving chromaticity mapping */

/* Get luminance component from $\mathbf{c}$ */

$Y \leftarrow c_2$;

/* *Transform to CIE $u'v'$ representation*: */

$(u_{\mathbf{c}}, v_{\mathbf{c}}) \leftarrow$CIE $u'v'$ chromaticities of $\mathbf{c}$;

$(u_{\mathbf{w}}, v_{\mathbf{w}}) \leftarrow$CIE $u'v'$ chromaticities of $\mathbf{w}$;

forall $i = 1,2,\ldots K$ **do**

  $(u_i, v_i) \leftarrow$CIE $u'v'$ chromaticities of $\mathbf{p}_i + \mathbf{p}_0$;

end

if $(u_{\mathbf{c}}, v_{\mathbf{c}})$ *is outside the polygon enclosed by channel chromaticities* $\{(u_i, v_i)\}_{i=1}^{K}$ **then**

  $(u_{\tilde{\mathbf{c}}}, v_{\tilde{\mathbf{c}}}) \leftarrow$ Intersection between the polygon and line-segment $(u_{\mathbf{c}}, v_{\mathbf{c}}) - (u_{\mathbf{w}}, v_{\mathbf{w}})$;

else

  $(u_{\tilde{\mathbf{c}}}, v_{\tilde{\mathbf{c}}}) \leftarrow (u_{\mathbf{c}}, v_{\mathbf{c}})$;

end

$\tilde{\mathbf{c}} \leftarrow$ XYZ tristimulus with luminance Y and chromaticity $(u_{\tilde{\mathbf{c}}}, v_{\tilde{\mathbf{c}}})$;

/* Stage II: Adjust "luminance" approx. preserving chromaticity */

/* Use Algo. 2 to compute pyramidal cone representation */

$\tilde{\boldsymbol{\alpha}}, \chi \leftarrow$ output from Algorithm 2 for target color $\tilde{\mathbf{c}}$;

if $\chi = 0$ **then**

  /* Some $\tilde{\alpha}_i < 0$, map to display black */

  $\hat{\boldsymbol{\alpha}} \leftarrow \mathbf{0}$;

else if $\tilde{\boldsymbol{\alpha}} \neq \mathbf{0}$ **then**

  /* If required scale down control values to make them feasible. Approximately preserves $u'v'$ chromaticity. */

  $\hat{\boldsymbol{\alpha}} \leftarrow \tilde{\boldsymbol{\alpha}} / \max[1, \max(\tilde{\boldsymbol{\alpha}})]$;

end

$\hat{\mathbf{c}} \leftarrow \mathbf{P}\hat{\boldsymbol{\alpha}} + \mathbf{p}_0$;

in the cone $\bar{Q}^{klm}$ and, as a result, we can find a representation for $\tilde{\mathbf{c}}$ in the form of Eq. (23) where $0 \leq \beta, \xi \leq 1$, and $1 \leq \nu$, where the last condition arises from the fact the $\tilde{\mathbf{c}}$ is outside Q^{klm}. Algorithm 2 provides equivalent information in the form of a nonnegative vector $\tilde{\boldsymbol{\alpha}}$ such that $\tilde{\mathbf{c}} = \mathbf{p}_0 + \mathbf{P}\tilde{\boldsymbol{\alpha}}$ where $0 \leq \tilde{\boldsymbol{\alpha}}$ and $\nu = \max(\tilde{\boldsymbol{\alpha}}) > 1$. While $\tilde{\boldsymbol{\alpha}}$ is not a feasible control value, the control value $\hat{\boldsymbol{\alpha}} = \tilde{\boldsymbol{\alpha}}/\nu$ represents the feasible control value such that $\hat{\mathbf{c}} = \mathbf{p}_0 + \mathbf{P}\hat{\alpha} = \mathbf{p}_0 + (1/\nu)\mathbf{P}\tilde{\boldsymbol{\alpha}}$ represents the in-gamut color to which $\tilde{\mathbf{c}}$ is mapped. From this mathematical expression, we can also immediately see the geometric relation shown in Fig. 14: the process translates $\tilde{\mathbf{c}}$ along the line segment joining $\tilde{\mathbf{c}}$ with the display black chromaticity $\mathbf{p}_0$ to the point where this line-segment intersects with the base of the quadrangle pyramid Q^{klm} and this intersection defines the gamut mapped point $\hat{\mathbf{c}}$. In the absence of flare ($\mathbf{p}_0 = \mathbf{0}$) and this process alters only the luminance, completely preserving chromaticity. In the presence of a small amount of flare, it is approximately chromaticity preserving. Based on the aforementioned description, the complete gamut mapping procedure (including both stages) is summarized in Algorithm 3, which also takes into account cases where the color is inside the gamut.

Acknowledgments

We thank the Center for Integrated Research Computing (CIRC), University of Rochester, for providing access to computational resources for this research.

References

1. International Telecommunications Union Recommendation BT. 2020-2, "Parameter values for UHDTV systems for production and international programme exchange," 2015, https://www.itu.int/rec/R-REC-BT.2020/ (April 2017).
2. S. Wen, "A method for selecting display primaries to match a target color gamut," *J. Soc. Inf. Disp.* **15**(12), 1015–1022 (2007).
3. K. Masaoka, Y. Nishida, and M. Sugawara, "Designing display primaries with currently available light sources for UHDTV wide-gamut system colorimetry," *Opt. Express* **22**(16), 19069–19077 (2014).
4. C. E. Rodríguez-Pardo et al., "Optimal gamut volume design for three primary and multiprimary display systems," *Proc. SPIE* **8292**, 82920C (2012).
5. K. Hirai, D. Irie, and T. Horiuchi, "Multi-primary image projector using programmable spectral light source," *J. Soc. Inf. Disp.* **24**(3), 144–153 (2016).
6. M. D. Fairchild and D. R. Wyble, "Mean observer metamerism and the selection of display primaries," in *Color and Imaging Conf.*, pp. 151–156, Society for Imaging Science and Technology, Albuquerque, New Mexico (2007).
7. R. Ramanath, "Minimizing observer metamerism in display systems," *Color Res. Appl.* **34**(5), 391–398 (2009).
8. D. Long and M. D. Fairchild, "Reducing observer metamerism in wide-gamut multiprimary displays," *Proc. SPIE* **9394**, 93940T (2015).
9. S. Wen, "Power-saving primary design for displays enclosing a target color gamut," *J. Soc. Inf. Disp.* **16**(11), 1131–1137 (2008).
10. C. E. Rodríguez-Pardo, G. Sharma, and X.-F. Feng, "Primary selection for uniform display response," *Proc. SPIE* **9015**, 90150I (2014).
11. L. Beke et al., "Optimal color primaries for three- and multiprimary wide gamut displays," *J. Electron. Imaging* **17**(2), 023012 (2008).
12. H. Xie, C. E. Rodríguez-Pardo, and G. Sharma, "Pareto optimal primary designs for color displays," *Electron. Imaging* **2017**(18), 84–90 (2017).
13. CIE, "Colorimetry," CIE Publication No. 15.2, Central Bureau of the CIE, Vienna, Austria (1986).
14. M. Kriss and P. Green, *Color Management: Understanding and Using ICC Profiles*, Vol. **17**, John Wiley & Sons, Chichester, West Sussex, England (2010).
15. T. Ajito et al., "Color conversion method for multiprimary display using matrix switching," *Opt. Rev.* **8**(3), 191–197 (2001).
16. M. Takaya et al., "Color-conversion method for a multi-primary display to reduce power consumption and conversion time," *J. Soc. Inf. Disp.* **13**(8), 685–690 (2005).
17. P. Centore, "Minimal-energy control sequences for linear multi-primary displays," *J. Imaging Sci. Technol.* **59**(5), 050502 (2015).

18. F. Konig et al., "A multiprimary display: optimized control values for displaying tristimulus values," in *Proc. IS&T/SID PICS 2002: Image Processing, Image Quality, Image Capture Systems Conf.*, pp. 215–220, Society for Imaging Science & Technology (2002).
19. D.-W. Kang et al., "Multiprimary decomposition method based on a three-dimensional look-up table in linearized lab space for reproduction of smooth tonal change," *J. Imaging Sci. Technol.* **50**(4), 357–367 (2006).
20. C. E. Rodríguez-Pardo and G. Sharma, "Multiprimary display color calibration: a variational frame-work for robustness to device variation," in *IS&T Electronic Imaging*, pp. 1–7, Society for Imaging Science and Technology, San Francisco, California (2016).
21. M. Yamaguchi, H. Haneishi, and N. Ohyama, "Beyond red–green–blue (RGB): spectrum-based color imaging technology," *J. Imaging Sci. Technol.* **52**(1), 010201 (2008).
22. Y. Murakami et al., "Color conversion method for multi-primary display for spectral color reproduction," *J. Electron. Imaging* **13**(4), 701–708 (2004).
23. T. Uchiyama et al., "A visual evaluation of the image reproduced on a multiprimary display by color decomposition based on spectral approximation," *J. Imaging Sci. Technol.* **49**(4), 410–417 (2005).
24. J. Morovič, *Color Gamut Mapping*, John Wiley & Sons, Chichester, West Sussex, England (2008).
25. J. Morovic, "Gamut mapping," Chapter 10 in *Digital Color Imaging Handbook*, G. Sharma, Ed., CRC Press, Boca Raton, Florida (2003).
26. C. E. Rodríguez-Pardo et al., "Efficient computation of display gamut volumes in perceptual spaces," in *Proc. IS&T/SID Nineteenth Color and Imaging Conf.: Color Science and Engineering Systems, Technologies, and Applications*, San Jose, California, pp. 132–138 (2011).
27. D. L. Long and M. D. Fairchild, "Modeling observer variability and metamerism failure in electronic color displays," *J. Imaging Sci. Technol.* **58**(3), 030402 (2014).
28. D. L. Long and M. D. Fairchild, "Observer metamerism models and multiprimary display systems," *SMPTE Motion Imaging J.* **125**(3), 18–29 (2016).
29. CIE, "Special metamerism index: change in observer," CIE Publication 80, Central Bureau of the CIE, Vienna, Austria (1989).
30. K. Deb, "Multi-objective optimization," in *Search Methodologies*, E. K. Burke and G. Kendall, Eds., pp. 403–449, Springer, New York (2014).
31. Y. Asano, *Individual Colorimetric Observers for Personalized Color Imaging*, PhD Thesis, Rochester Institute of Technology (2015).
32. CIE, "Recommended practice for tabulating spectral data for use in colour computations," CIE Publication No. 167, Central Bureau of the CIE, Vienna, Austria (2005).
33. H. J. Trussell and M. S. Kulkarni, "Sampling and processing of color signals," *IEEE Trans. Image Process.* **5**, 677–681 (1996).
34. G. Sharma and H. J. Trussell, "Decomposition of fluorescent illuminant spectra for accurate colorimetry," in *Proc. IEEE Int. Conf. Image Processing (ICIP '94)*, Vol. **2**, pp. 1002–1006 (1994).
35. K. Deb et al., "A fast and elitist multiobjective genetic algorithm: NSGA-II," *IEEE Trans. Evol. Comput.* **6**(2), 182–197 (2002).
36. M. H. Brill et al., "Prime colors and color imaging," in *Color and Imaging Conf.*, pp. 33–42, Society for Imaging Science and Technology, Scottsdale, Arizona (1998).
37. G. Sharma and C. E. Rodríguez-Pardo, "The dark side of CIELAB," *Proc. SPIE* **8292**, 82920D (2012).
38. International Telecommunications Union Recommendation BT. 709-6, "Parameter values for the HDTV standards for production and international programme exchange," 2015, https://www.itu.int/rec/R-REC-BT.709/ (April 2017).
39. K. Masaoka, "Analysis of standard chromaticity gamut area metrics," *J. Soc. Inf. Disp.* **24**(12), 741–746 (2016).
40. K. Masaoka, "Display gamut metrology using chromaticity diagram," *IEEE Access* **4**, 3878–3886 (2016).
41. H. Xie, C. E. Rodríguez-Pardo, and G. Sharma, "Pareto optimal color display primary design (project webpage)," http://www.ece.rochester.edu/gsharma/ParetoOptimPrimDesign/ (May 2017).
42. C. E. Rodríguez-Pardo and G. Sharma, "Calibration sets for multiprimary displays: representation, visualization, and applications," in *Proc. IS&T/SID 22nd Color and Imaging Conf.*, Boston, Massachusetts, pp. 171–179 (2014).
43. P. Centore and M. H. Brill, "Extensible multi-primary control sequences," *J. Soc. Inf. Disp.* **20**(1), 12–21 (2012).
44. H. Coxeter, *Regular Polytopes*, Dover Publications, New York (1973).

Hao Xie is a graduate student in the Electrical and Computer Engineering Department at the University of Rochester, where he is currently pursuing his master of science (MS) degree. He received his BEng degree in information engineering from Zhejiang University, China. His research interests include color science and computational photography.

Carlos Eduardo Rodríguez-Pardo received his BS and MS degrees in electronics engineering from the Universidad de los Andes, Bogota, Colombia, and his MS degree in electrical and computer engineering from the University of Rochester, Rochester, New York, USA, where he is currently a PhD student. His research interests lie in the area of color imaging, the human visual system, and image processing. He is a student member of SPIE, IS&T, and IEEE.

Gaurav Sharma is a professor at the University of Rochester in the Department of Electrical and Computer Engineering, in the Department of Computer Science, and in the Department of Biostatistics and Computational Biology. He is the editor of the *Color Imaging Handbook*, published by CRC Press in 2003. He is a fellow of SPIE, of the Society of Imaging Science and Technology (IS&T), and of the IEEE, and a member of Sigma Xi.